Project Number: MQP NAB MQP7

Lateral Force Calibration for Probe Microscopy

A Major Qualifying Project Report

submitted to the Faculty

of the

WORCESTER POLYTECHNIC INSTITUTE

in partial fulfillment of the requirements for the

Degree of Bachelor of Science

by

Colin DeGraf

Keeley Stevens

Date: April 26, 2007

Approved:

Professor Nancy Burnham, Advisor

Abstract

To improve the measurement of nanoscale friction, a new alternate method of lateral calibration for the atomic force microscope was examined. This method, which offers the advantage of reduced tip wear, was reviewed and analyzed, and fundamental flaws were identified in its derivation. After modifying this approach, we attempted to confirm our corrected model with a commonly accepted calibration method. The collected data displayed as yet unexplained oscillatory behavior, which showed strong correlations between lateral, drive, and error signals.

Acknowledgements

We would like to acknowledge and thank Professor Nancy A. Burnham for her invaluable guidance and help throughout this project. We would also like to thank Dr. Deli Liu and all of the Physics Department at WPI for their support in this project, which was graciously funded by a Grant-In-Aid of Research from Sigma Xi, The Scientific Research Society.

Table of Contents

Table of Figures

1 Introduction

At the most basic level, physics is built upon knowledge of the forces acting within any given system across a range of scales. For cutting edge science on the nanoscale, this is far from a trivial problem, especially in mechanical systems such as in micro-electro-mechanical systems. This project focuses upon the development of an improved system of calibration for the measurement of lateral forces, such as friction, using an atomic force microscope (AFM).

Atomic force microscopy is a unique method of characterizing many of the properties of a sample. The term "microscopy" can be misleading, as an atomic force microscope (AFM) does not use light to capture an image. Instead, it senses the surface in a similar way as a blind man might read braille text by running his finger across the surface features. An AFM uses a nanometer-scale version of the man's finger, the cantilever, to move across the surface and collect data. This cantilever, the crucial element of the AFM, is typically on the order of 200 μm in length and 20 μm in width, and is controlled by a piezo drive system within the scan head. A laser is reflected off the end of the cantilever, and the reflected beam hits a photodetector (Figure 1). The position of the beam on the photodetector is registered, and the allowing the displacement of the beam to be calculated. Since the reflected beam is displaced more than the cantilever, the position of the cantilever can be known to a high degree of accuracy. [17]

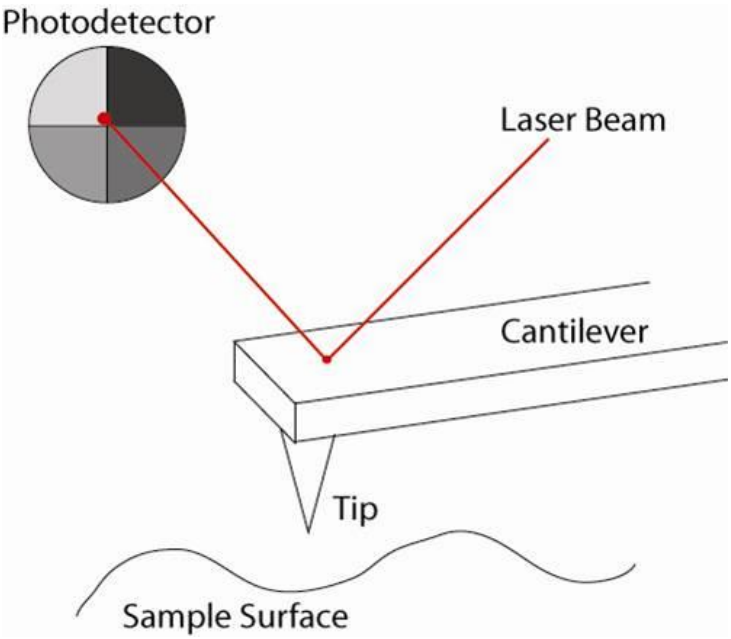

Figure 1: Reflection of laser off cantilever before hitting the photodetector.

This "nano-finger" can be used in a number of different modes to collect surface data; for smooth surfaces, it can simply be slid across the surface, in what is known as contact-mode imaging. For rough samples, intermittent-contact imaging may be used, where the "finger" taps along to collect height data at regular intervals. If the surface has magnetic properties, non-contact mode imaging may be used where the cantilever is kept a constant distance from the surface and any deflection in the beam indicates the presence of an attractive or repulsive field. The cantilever may also be used to measure lateral forces (most commonly friction on the surface of the sample) by looking closely at the twist of the cantilever. In the specific case of friction, the observed twist can be used to find the static friction before the tip begins to slide, and also at the kinetic friction after the tip begins to slide across the surface (Figure 2). There are many other ways in which an AFM can be used, including manipulating samples down to the atomic scale, and measuring other physical properties of samples. One crucial piece of information which must be known to perform these analyses is the cantilever force-constant: the

force required the cause the cantilever to bend by a certain amount, both normally and laterally. Only with this knowledge can the actual values of the data obtain be found, and it is the calibration of this lateral force-constant that is the focus of our project.

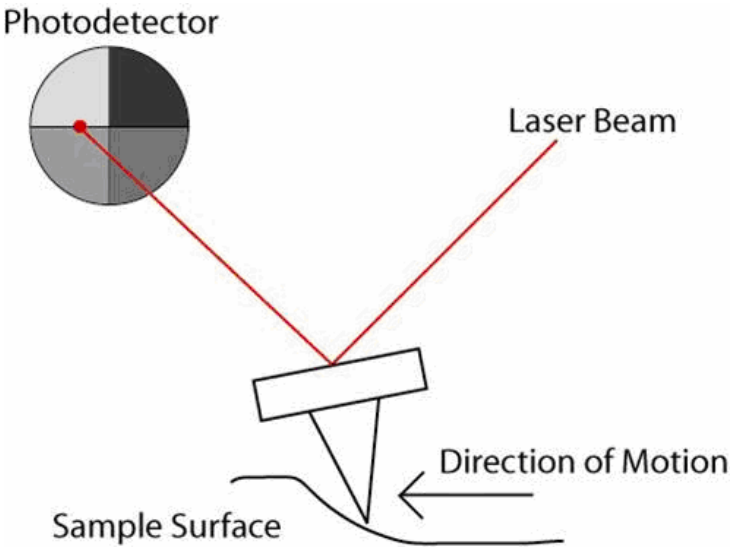

Figure 2: AFM used to measure lateral forces, by observing the twisting due to the lateral forces on the tip

Our central goal was to analyze and critique a newly proposed method for lateral calibration, which presents numerous advantages, primarily that it reduces tip wear on the AFM. Upon investigation, numerous flaws were identified stemming from a range of assumptions, which were then reviewed and a new model was presented. Our intention was then to produce experimental data demonstrating the flaws in the proposed method while validating our newly derived equations based upon a different set of assumptions.

Unfortunately, even after several problems in the experimental design were overcome, the collected data were substantially different from what was expected, such that they could not be used for calibration. As a result, much of the later portion of the project was spent investigating the unexpected oscillatory behavior found in our data. The time constraints on the project regrettably prevented the development of a conclusive theory for this behavior; however,

significant progress was made towards such an explanation, and the groundwork was laid for future research to complete the goals set forth at the beginning of this project.

In the following sections, a detailed account of the background for this project is given, particularly the current status of lateral force calibration. This is followed by the initially proposed methodology to obtain desired results, and a detailed account of this process, as well as the additional work done in an attempt to explain the results. Finally, conclusions as to the success of the project are given, followed by appendices enumerating the detailed steps needed to reproduce our data, and the data itself.

2 Studies of Friction at the Nanoscale

Friction has been extensively studied on the macroscale, and its behavior is reasonably well understood. Specifically, Amonton's Law specifies that the force of friction is proportional to the load force applied, and independent of the contact area [1]:

$$F_f = \mu F_N$$

In the mid 20th century, Bowden and Tabor proposed that the frictional force is actually proportional to the true contact area between asperities of the surface (though not dependant upon the overall contact area between surfaces)[2]. In turn, if one assumes that the contact area is based upon plastic deformation, one finds that the true contact area (A) is proportional to the load force (F_N), and thus one obtains Amonton's Law again[2]:

$$A \propto F_N \qquad F_f \propto A$$

$$\text{and so } F_f \propto F_N$$

A problem arises when one begins to consider that the contact area does not depend solely on plastic deformation. Israelachvili verified that friction was indeed proportional to the contact area, and not only that, but the relation held true even in the absence of wear[3]. This implied that the contact area cannot be determined simply by plastic deformation. One can also incorporate elastic deformation and use Hertzian mechanics, which results in a relation of

$$A \propto F_N^{2/3}. \text{ [4]}$$

This is problematic, as it results in an unclear relation between contact area and load force. Greenwood and Williamson found that for certain distributions of asperities (including exponential and Gaussian), $A \propto F_N$, which verifies that in Amonton's Law holds for the macroscale.[2]

However, at the nanoscale, there are additional problems. Modeling the interactions with Hertzian mechanics is reasonable in certain cases, (which gives the result $A \propto F_N^{2/3}$ as considered above), but it does not account for adhesion forces. This is of limited accuracy, however, since at the nanoscale, the adhesion forces are non-trivial, and thus should not be ignored. Both JKR and DMT models can be used, which each account for different types of adhesion. These different results can be seen in the following figure:

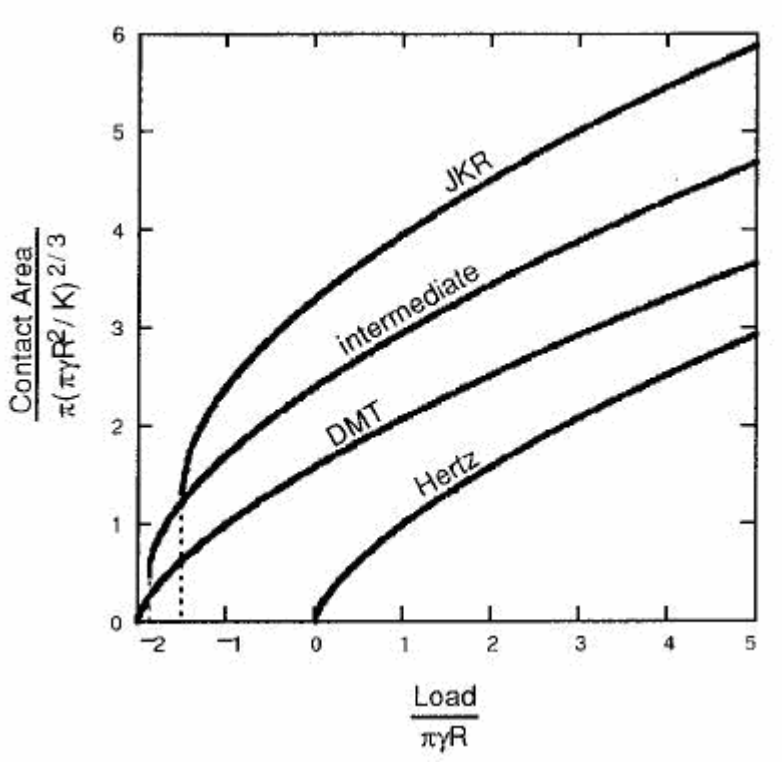

Figure 3 [4]**:** Relationship between load and contact area for varying models of adhesion

As such, there are many different ways to model the frictional force as a function of the contact area, and the contact area as a function of the load, where the most accurate model depends on the tip and sample being used. While some tip-sample interactions follow substantially non-linear behavior, as in Figure 4, others follow a linear relationship (Figure 5),

which can be modeled by a modified version of Amonton's Law, which has a vertical offset based upon the adhesive force A[5]:

$$F_f = \mu(F_N + A)$$

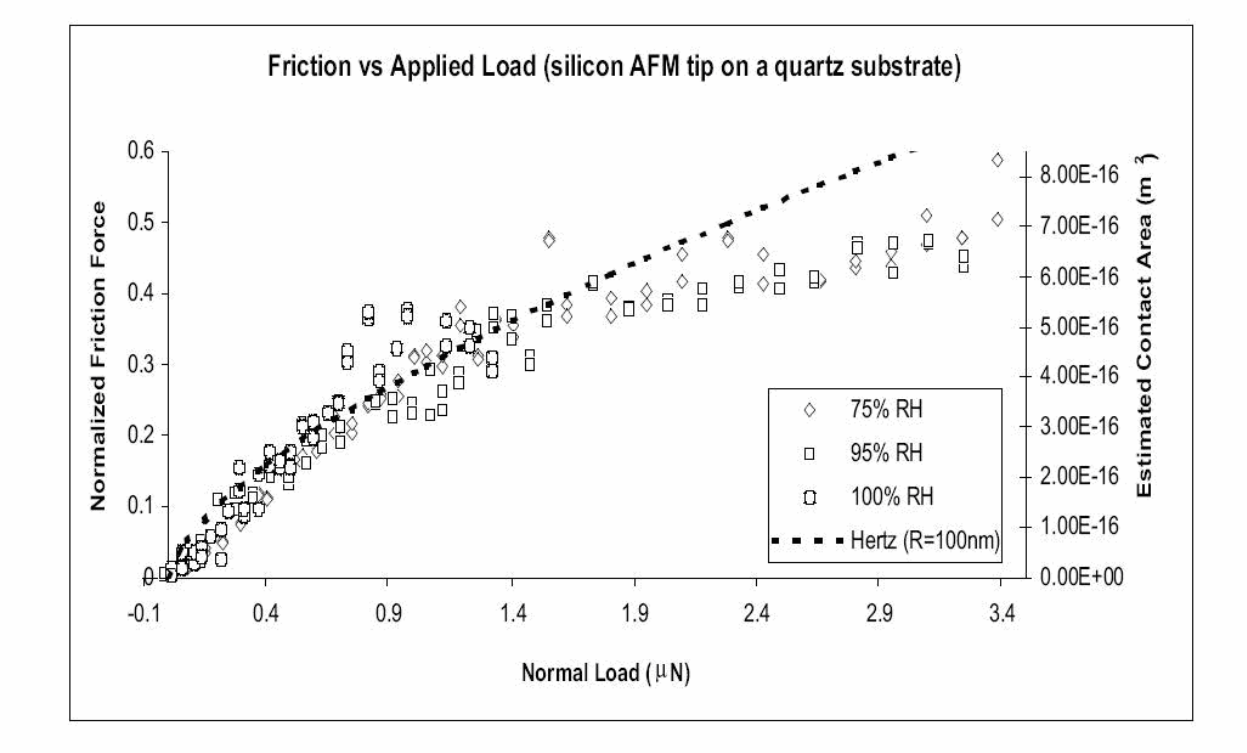

Figure 4 [1]: Nonlinear relationship between normal load and contact area/frictional force

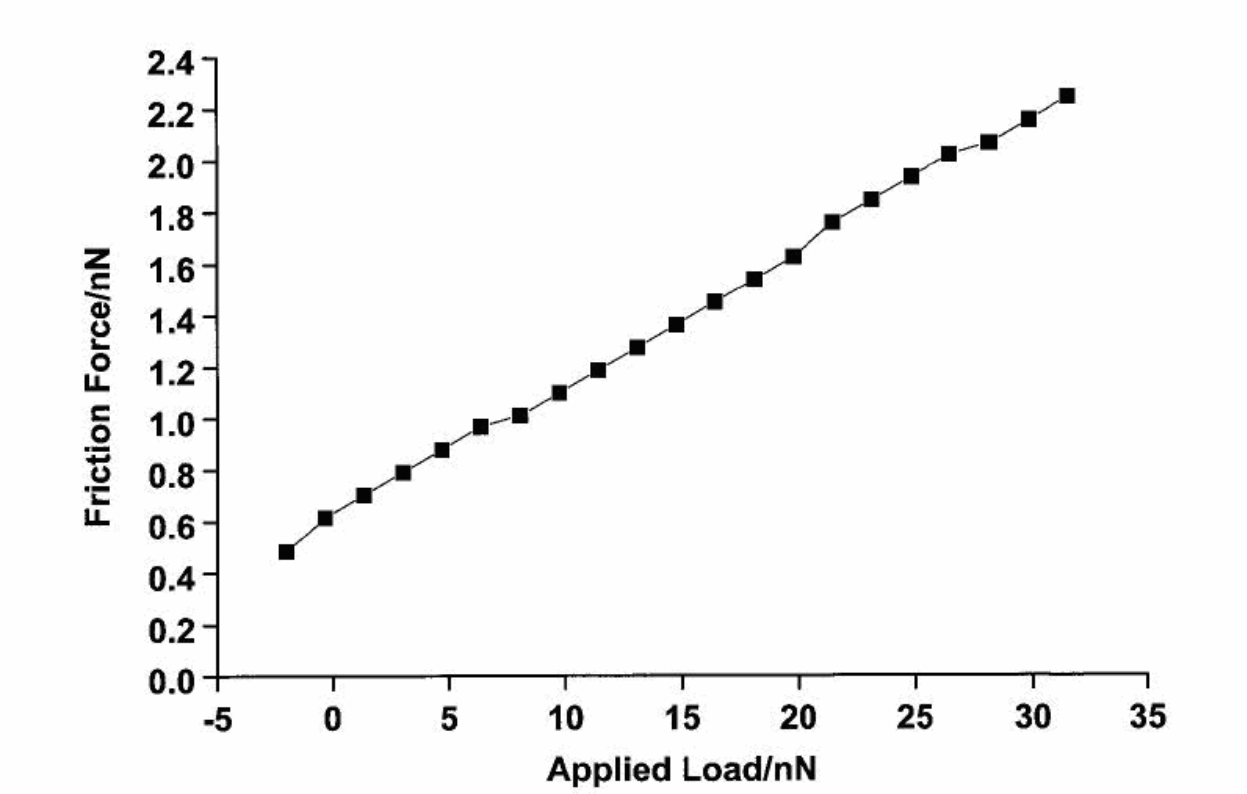

Figure 5 [5]**:** Demonstrated linear behavior of normal force versus frictional force curve

Due to the wide discrepancies between results based upon different theories of contact mechanics, it is necessary to take experimental data for the tip-sample interactions that are to be used and experimentally determine which, if any, of the above relations is most accurate for any given experiment.

2.1 Major Methods in Lateral Calibration

In order to study friction at the nano-scale, it is necessary to take very accurate measurements of extremely small forces. An atomic force microscope is well suited to work on this scale, and the development of lateral force microscopy has made these frictional measurements possible.

2.1.1 Mate's 1987 Initial Investigation of Nano-scale Friction

The study of lateral force calibration began in 1987, when Mate [6] published initial findings of lateral friction using an atomic force microscope. By dragging a tungsten wire tip across a cleaved graphite surface, he observed slippage consistent with the atomic structure of graphite. As he increased the load upon the wire tip, the magnitude of the frictional force tended to increase. This force was also periodic, correspondent to the surface features of the basal graphite plane being scanned.

As this introduced the study of frictional force measurement, calibration was limited to the basic macroscopic model of friction. It was noted as a purely linear force, although nonlinear deviations were noted. Mate stated that there was a great deal of research still to be done to understand the dynamics of this interaction.

Many of the intricacies that are the focus of more modern research were introduced by Mate. He noted the relationship between contact area and deformation, along with the inclusion of asperities in the tip. Nonlinearities in the measurement of frictional force were attributed to unexpected interactions of asperities. By studying mica, he also noted an atomic-level "slip-stick" pattern to the force measurements. This slip-stick pattern is of great interest, between the static and dynamic modes of surface friction.

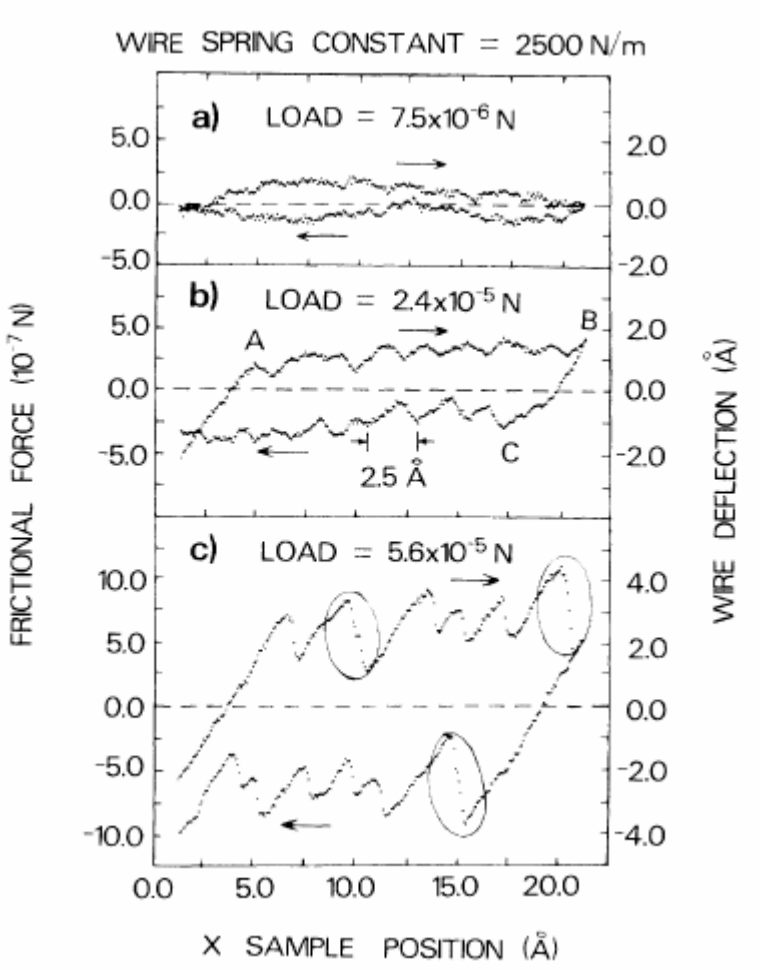

Figure 6 [6]**:** Relationship of frictional force and wire beam deflection over varying normal loads on a graphite sample

2.1.2 Ruan and Bhushan's 1994 Calibration Method

Throughout the next decade, lateral forces in the AFM became a popular subject. In 1994, Ju-Ai Ruan and Bharat Bhushan worked to develop a calibration procedure for commercial AFM systems capable of measuring lateral forces [7]. They proposed two methods of calibration which use complimentary techniques to calculate the frictional force applied to the cantilever and the coefficient of friction on the surface.

Their first method is a very straightforward technique. By taking standard topography images forward and backward while scanning parallel to the cantilever beam, the force applied to the base of cantilever to maintain a constant flexure is directly related to the frictional force applied to the tip. As frictional force acts opposite the motion of the scan, reversing the direction allows this frictional contribution to be quantified. If the absolute value of the normal force applied to the cantilever is recorded at every point on a scanline, this can be combined with the length and tilt of the cantilever to produce a value of the coefficient of friction.

There are many sources of error within this method. Adhesive and/or interatomic forces at the surface affect this simple approach to the total forces on the tip. Often, these are small enough to be ignored, but this assumption can lead to large uncertainties. This method also relies heavily on the assumption that the friction force is independent of the scanning direction. Experimentally, scanner hysteresis can add uncertainty to the final measurement, making this method a poor choice for an in-depth study, but useful as a check for other lateral calibration methods.

Ruan and Bhushan offer a second, more accurate method in their paper based on the lateral bending of the cantilever during perpendicular scans. As the cantilever twists during these scans, the shift in the lateral position of the laser beam on the photodetector shifts measurably. Friction is not the only factor contributing to the flexure of the cantilever, but this can be accounted for. When the cantilever is in contact with the surface but not scanning, there are no lateral forces being applied to the tip. Thus, any lateral signal from the photodetector while the tip is stationary can be ruled out from dynamic measurements. By once again scanning in forward and backward directions, the averaged value produces a much more reliable value for the coefficient of friction than their first method.

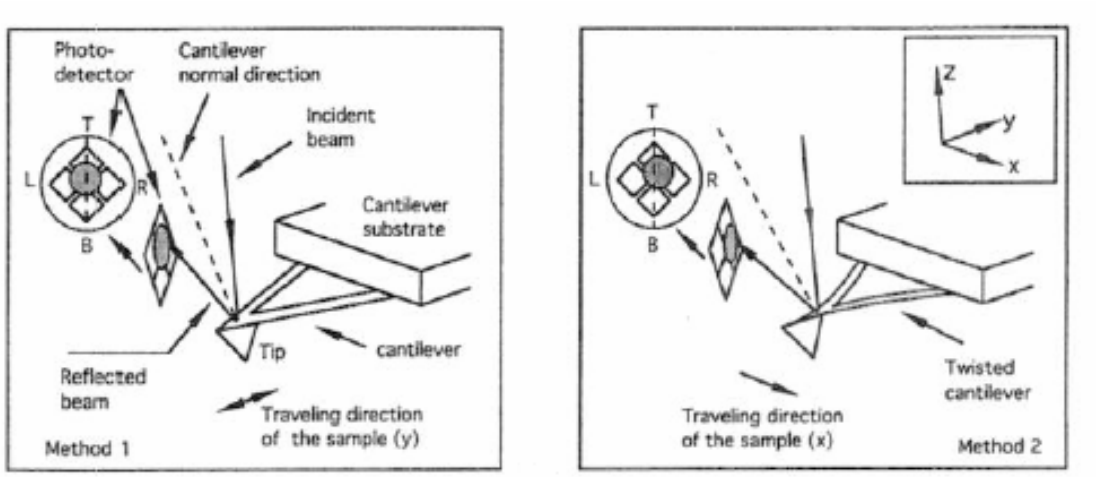

Figure 7 [7]**:** Diagram of laser displacement on photodiode for parallel and perpendicular scan directions

It is worth noting that both of these methods require a firm knowledge of the normal force applied to the surface. To do this, a separate calibration is needed to determine the spring constant of the cantilever. This subject is much better understood today than it was in 1994 when Ruan and Bhushan authored their paper. Classic geometrical approximations can be highly erroneous, partially due to large variances in the materials used for cantilevers. The equations for this geometric approach used by Ruan and Bhushan depend strongly on the thickness of the cantilever, following the cube of the thickness. As this measurement is quite difficult, errors are easily introduced. Sader has since introduced a widely accepted method of calibrating the normal spring constant [8] which requires no modifications to the cantilever or tip, nor does it depend on measurements of the beam. This method is considered very accurate and is used commercially to calibrate the spring constant of many manufactured cantilevers. An alternative approach is through thermal measurements of the resonance of a given cantilever, proven to be accurate to 10% [9].

2.1.3 Ogletree, Carpick and Salmeron's 1996 Calibration Method

In 1996, D.F. Ogletree, R.W.Carpick and M. Salmeron [10] published a method of lateral calibration based on repeated scans of angled surfaces. This is a well accepted experimental method which builds off the second method introduced by Ruan and Bhushan. In practice, there are many sources of error which can affect the lateral twist of the cantilever and the resulting signal from the photodetector. Alignment is crucial to the accuracy of the Ruan method: alignment of the laser on the cantilever, alignment of the reflected light onto the photodetector, and the verticality of the photodetector relative to the system. Ogletree et al. propose scanning across sloped surfaces to eliminate the cross-talk errors caused by these misalignments within the system.

To obtain accurate, known slopes suitable for scanning, a $SrTiO_3$ (305) sample was used. This is unique as it readily forms compact +14.0 ° and -12.5 ° facets, allowing single scans to bridge multiple angles. By using a sample of known slopes, calibration of the motion of the Z piezo is simplified, as it can be adjusted until scans produce the correct angle between two slopes.

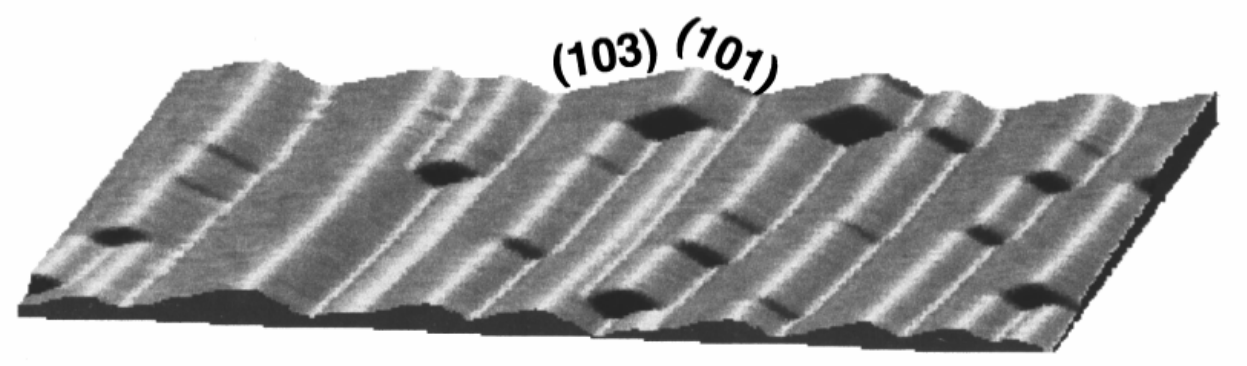

Figure 8 [10]**:** $SrTiO_3$ (305) surface, manufactured by Ogletree, Carpick and Salmeron to provide known angles of +14.0 ° and -12.5 ° on the nano-scale

On a known slope, the force equations become greatly simplified to the normal force from the tip, the horizontal driving force of the cantilever, and the frictional force. With these relationships at hand, data is collected by repeating a single scan line across multiple slopes while varying the normal force applied to the cantilever. This variation produces the data necessary to calibrate the lateral force signal.

2.1.4 Varenberg, Etsion and Halperin's 2003 Wedge Method Modifaications

While the method proposed by Ogletree et al. is widely accepted and cited, it relies on the obscure $SrTiO_3$ (305) surface shown in Figure 8. The dimensions on this sample prevent the use of many wider tips or colloidal sphere tips. The $SrTiO_3$ (305) surface is also unavailable to many, as there are no commercial manufacturers. Nearly a decade later, M. Varenberg, I. Etsion and G. Halperin worked through this method to adapt it for use on more readily available commercial calibration grating [11]. On the grating used by Ogletree et al. there was no flat surface on which to obtain a median lateral signal. Varenburg suggests the use of a silicon grating with (100) and (111) faces, which produced sections of 0° and ±54.44 °. The addition of the flat portions greatly simplifies the interpretation of the torsional signal while still producing values for the coefficient of friction which agree with published values. This is advantageous, as this Si (100) grating is commercially available, allowing many more labs to explore lateral force microscopy.

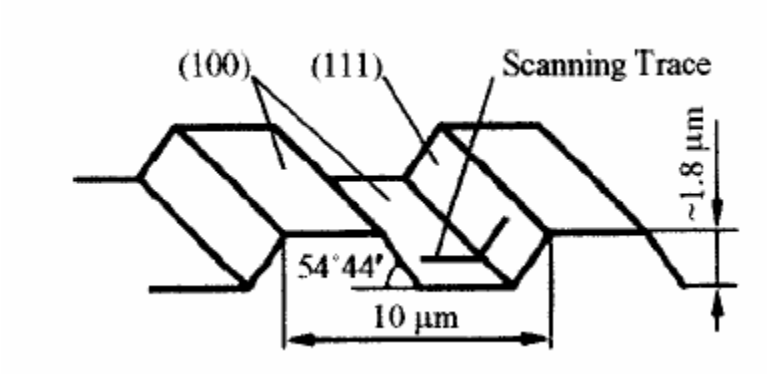

Figure 9 [11]**:** Commercially available 54.44° calibration grating used by Varenberg et al. for lateral calibration

2.1.5 Tocha, Schönherr and Vansco's 2006 Wedge Method Modifications

E. Tocha, H. Schönherr, and G. Vancso also build upon the method presented by Ogletree et al., but offer a universal specimen appropriate to a wider range of cantilever tips [12]. They note that the Si (100) specimen used by Varenberg et al. is appropriate for very sharp tips with long profiles, but the ±54.44° sides are steeper than many cantilever tips. This would lead to the side of the tip sliding up or down the side, nullifying any frictional data collected. Instead, they propose a sample of Si(100) fabricated using focused ion beam milling to produce angles of 20°, 25°, 30° and 35° relative to the surface. These were produced in a similar pattern to the wedge used by Varenberg et al., with flat notches of width 30-50µm and crests and sides with the specified angle. This sample is also durable, such that is may be cleaned with standard wafer cleaning techniques. With this, a wider variety of cantilever tips may be calibrated.

Aside from their contribution to the wedge calibration method, Tocha et al. present an exhaustive review of publications on the topic of friction at the nano-scale. This is a valuable resource as it points to many works related to specific issues within the field. They also include

a thorough review of factors that may affect wedge calibration accuracy, regardless of which wedge sample is in use.

2.3 Recent Advancements in Lateral Force Microscopy

As research in nano-scale friction continues, accepted methods of calibration are consistently reviewed, resulting in published papers confirming the methodology and offering small improvements. However, many researchers choose to develop new methods in lateral calibration, which often employ unique approaches to gain new insight into the problems of lateral force microscopy.

2.3.1 Reinstädtler's 2003 Torsional Resonance Calibration

With specialized equipment, tools such as a specific calibration grating may not be necessary. Reinstädtler et al. proposed a very different approach to lateral force calibration by driving the stage with a generated wave to induce torsional resonance in the cantilever [13]. The stage is fitted with a shear wave transducer, allowing the signal generator to adjust the frequency and magnitude of the induced waves. The cantilever beam behaves like a standard linear damped oscillator until higher amplitudes are reached by the driving system, when it appears that sliding friction occurs between the tip and the aluminum surface.

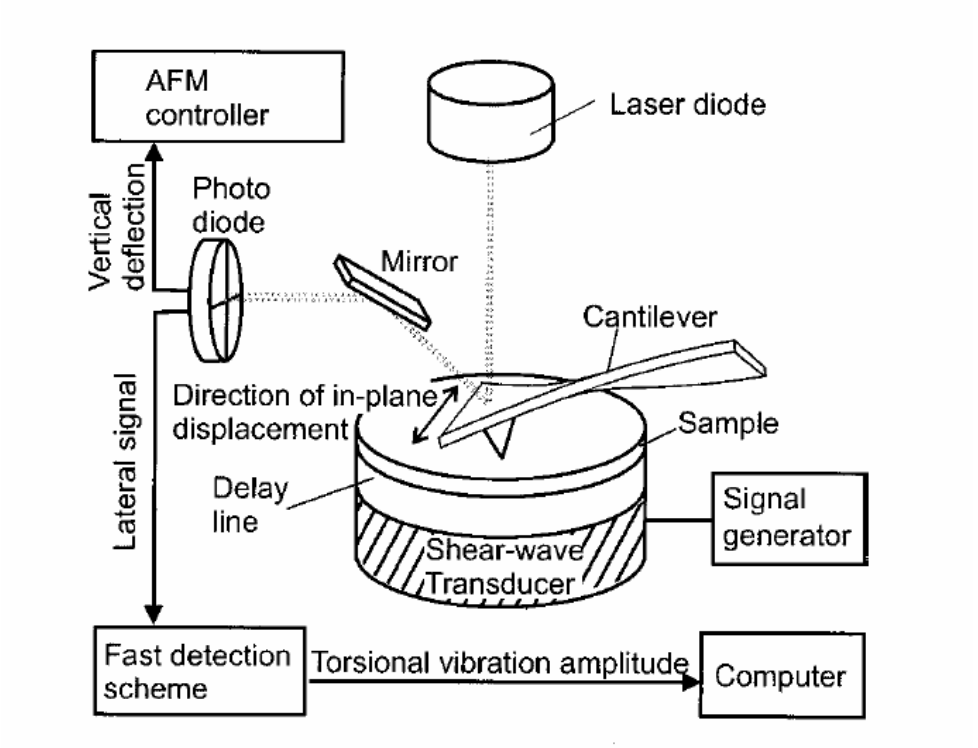

Figure 10 [13]**:** Experimental setup used by Reinstädtler et al. to induce vibrations in the cantilever, allowing calibration without surface scanning

2.3.2 Bilas' 2004 Piezotube Calibration

In certain situations, idiosyncrasies within a certain system might even be desirable to quantify lateral forces in a system. P. Bilas et al. introduce a method specific to atomic force microscopes which use a piezotube translator to drive the cantilever [14]. In these systems, as the piezotube extends to its maximum range, some bending occurs. This is amplified by the design of the system, where the cantilever extends off of the piezotube, leaving the tip offset from the axis of motion. This characteristic distortion is typically removed during image processing, but it can also be used as an advantage to couple the X-Y response to the Z response of the piezo. Using this and standard accepted calibrations for cantilever spring constants, quantitative frictional data can be obtained. While accurate, this is impractical when available equipment is not equipped with piezotube drivers for use with offset cantilevers.

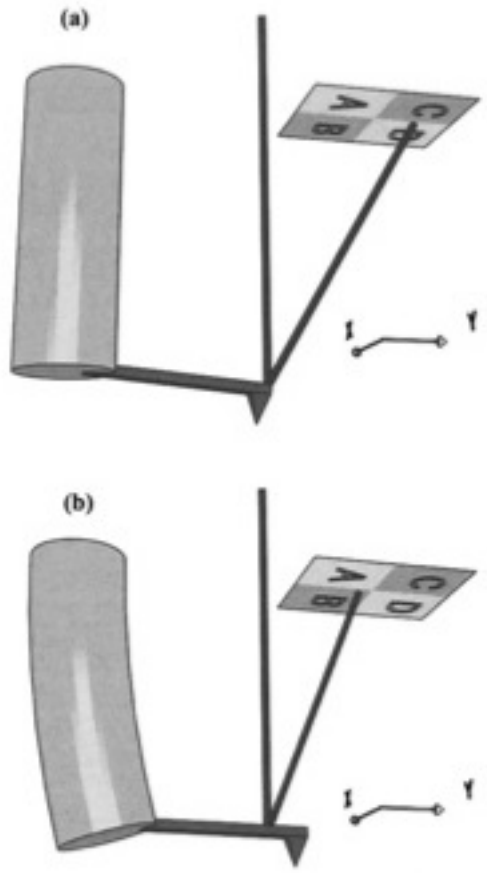

Figure 11 [14]**:** Piezotube deflection and its effect on laser position on photodiode as basis for the conclusions of Bilas et al.

2.4 Asay and Kim's 2006 Force Balance Calibration

A new method for finding the lateral calibration factor has been proposed by Asay and Kim [15]. This new 'force-balance method' relies on lateral force-distance curves taken on a calibration grating with known slopes (as shown in Figure 12). By finding the lateral deflection as a function of the load force and the angle of incline of the surface, one can calculate the lateral calibration factor for the cantilever being used, by writing equilibrium force equations, as in Figure 13.

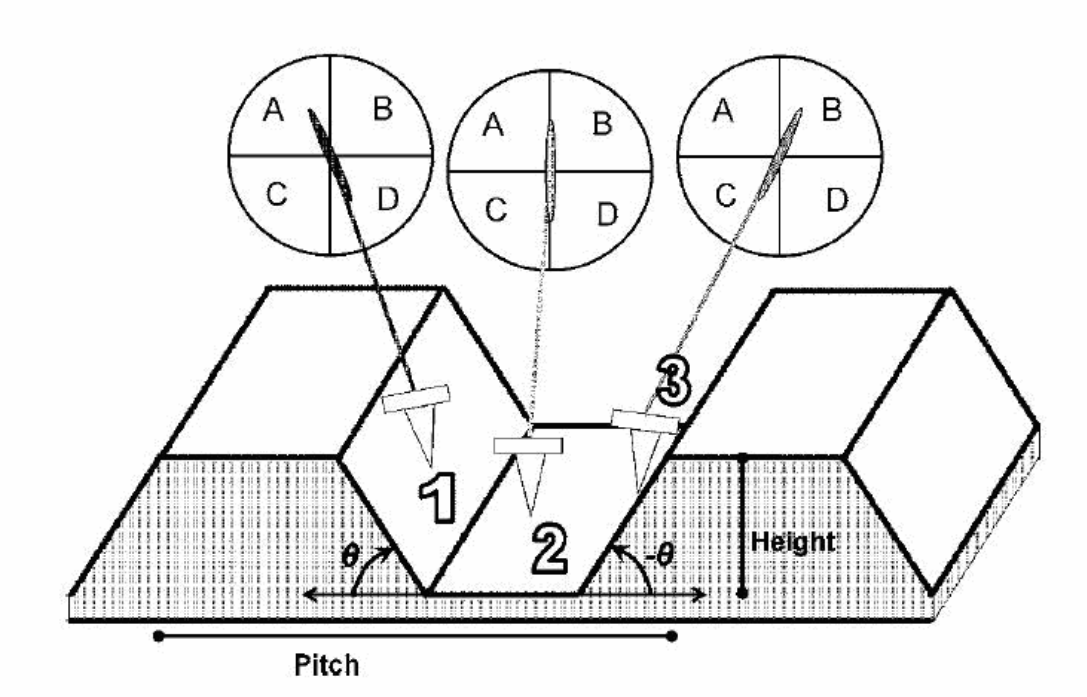

Figure 12 [15]**:** Path traced by the laser on the photodiode during lateral force curves on surfaces (1), (2), and (3)

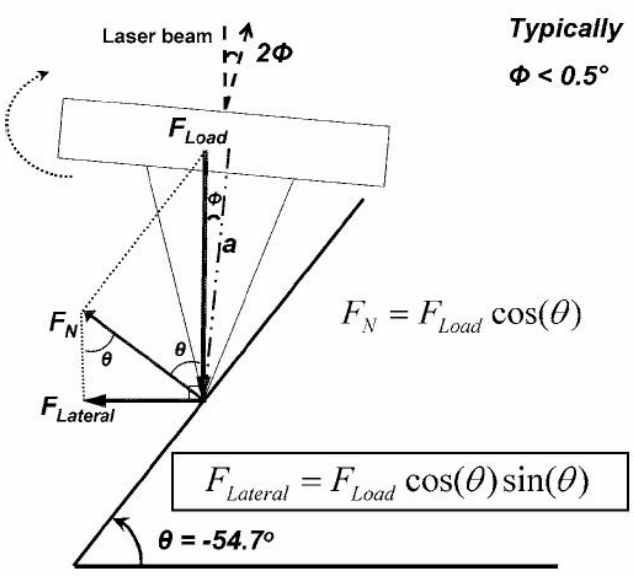

Figure 13 [15]**:** Force balance system used to derive Asay and Kim's expression for lateral force

Since the angle of incline is known and remains constant, one needs to simply take measurements of the normal force and the voltage from the lateral force, and substitute them into the equation

$$S_{Lateral} = \frac{F_{Lateral}}{V_{Lateral}}$$

$$\text{where } F_{Lateral} = F_{Load}\cos(\theta)\sin(\theta)$$

To get the measurements of the normal force and corresponding lateral force, one takes lateral force-distance curves for the three regions in Figure 12 with the resulting data displayed as in Figure 14:

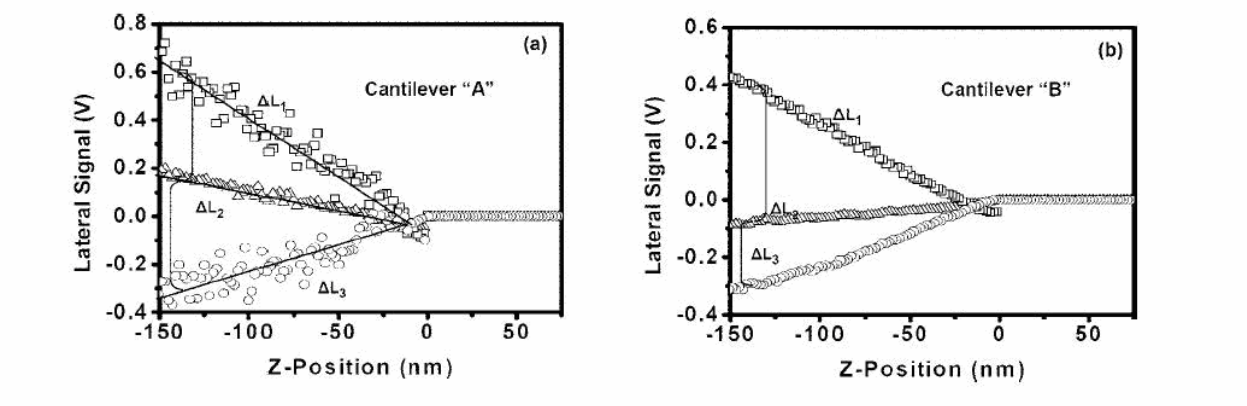

Figure 14(a) and (b) [15]**:** Comparison of lateral force curves collected on surfaces (1), (2), and (3). Figure (a) shows the symmetry present for an aligned photodetector, Figure (b) diagrams the effect of photodector misalignment.

If the photodetector on the AFM is not correctly aligned, there may be some cross-talk between the lateral signal and the vertical signal, in which case one averages the slopes of the lateral *f-d* curve on the sloped surfaces, as in Figure 14 (a), though the equations remain essentially unchanged.

If the AFM tip is placed off-center on the cantilever, then the equations must be adapted to account for the additional torque, as in Figure 15:

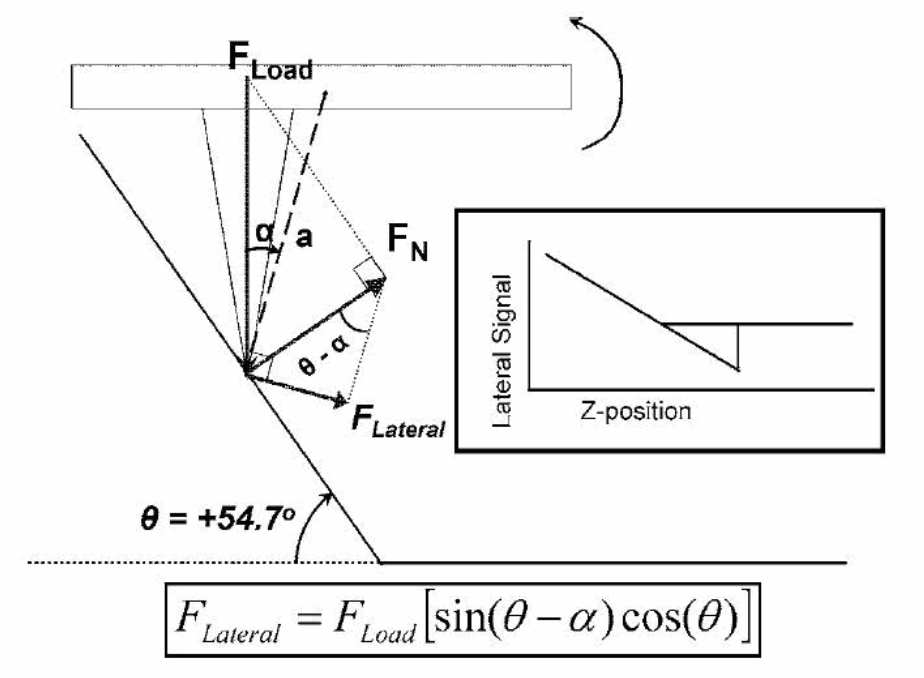

Figure 15 [15]**:** Modification to the force-balance system to account for torque due to an off-centered tip on the cantilever

In this case, one will obtain a lateral *f-d* curve as in Figure 14 (b). The slopes on all 3 surfaces (flat, and sloping each way) must be taken, and plugged into the equations

$$(\Delta D + \Delta L_1)S_{Lateral} \cong k_z[\cos(\theta)\sin(\theta-\alpha)]$$

$$(\Delta D + \Delta L_2)S_{Lateral} \cong k_z[-\sin(\alpha)]$$

$$(\Delta D + \Delta L_3)S_{Lateral} \cong k_z[\cos(-\theta)\sin(-\theta-\alpha)]$$

ΔD is the detector offset
α is the angle between the tip and the center of the cantilever
k_z is the normal spring constant of the cantilever

Clearly if the tip is off-centered, the equations become significantly more complicated, but in any of the three cases, one can take the necessary data to solve for the lateral calibration factor. The key advantage of this method over others is that it obtains the calibration factor without requiring taking repeated scans (as in the method published by Ogletree et al.), and thus minimizes the wear on both the tip and the calibration grating.

As outlined in this section, there are a number of accepted methods for lateral calibration. Asay and Kim's recently proposed method has notable advantages over some of its predecessors, but no method is without its downsides. There are a number of flaws made in the development of the method, leading to final equations which misrepresent the system. The initial focus of this project was the identification of these flaws and the necessary corrections to the method, as outlined in the following section.

3 Methodology

While the general idea behind the direct force-balance approach proposed by Asay and Kim (2006) seems valid, there are several problems with the way it is applied. Specifically, the equilibrium equations used to derive the final result of $F_{Lateral} = F_{Load}\cos(\theta)\sin(\theta)$ are incorrect. By looking at Figure 16, it is clear that there must be a problem, since there are three forces which clearly cannot sum to zero (despite the fact that they must sum to zero for equilibrium to hold). The source of this problem is that the $F_{Lateral}$ force is placed incorrectly. The authors' intent seems to be that $F_{Lateral}$ represents the lateral component of the overall forces, which is negated by the lateral force applied by the cantilever (henceforth termed F_x), whose magnitude is that required to balance the net lateral force (and we can see that F_{Load} is completely vertical, so only F_N has a lateral component). However, this change is not sufficient to completely fix the equations.

Even by replacing $F_{Lateral}$ with F_x (which points in the opposite direction), the forces will not properly balance. This is seen by considering the vertical forces. By simple geometry, we see that the normal force has a vertical component of $F_N\cos(\theta)$, and for the vertical forces to balance, this would have to be set equal to F_{Load}, as it is the only other force with a vertical component. This gives us the equation $F_N\cos(\theta) = F_{Load}$. However, we can also use the fact that the normal force arises from the load force, giving us the equation $F_{Load}\cos(\theta) = F_N$. Since these two equations relating F_{Load} and F_N are equivalent only for $\theta = 0$ (a flat surface), the free-body diagram is necessarily flawed. This can be fixed with the addition of two forces: static friction and adhesion (See Figure 17).

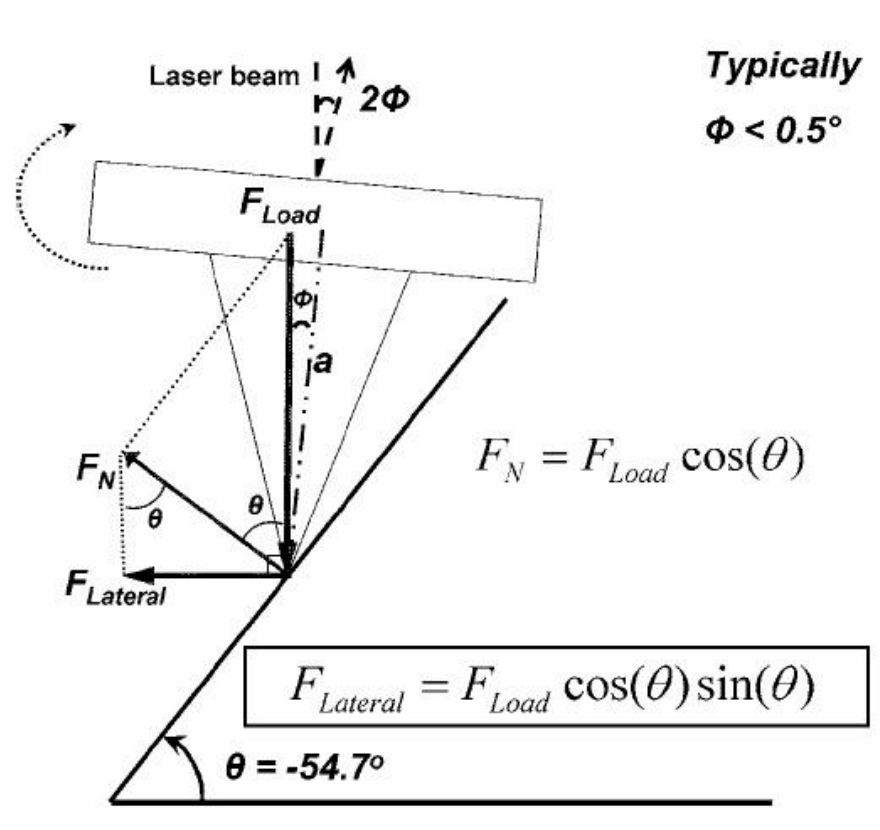

Figure 16 [15]**:** Asay and Kim's original free-body diagram

The primary force which is missing is the force of friction. We know that friction must play a role, since the method assumes that the force of friction is sufficient so as to prevent slipping, and thus it is important to model it. In addition, since we are dealing with a tip-sample interaction at the nanoscale, the force of adhesion may be substantial enough to require its addition. Thus we shall modify the free body diagram in Figure 16 to that displayed in Figure 17. We make the assumption that the twist of the beam, φ, is very small and can be disregarded (and is omitted in Figure 17).

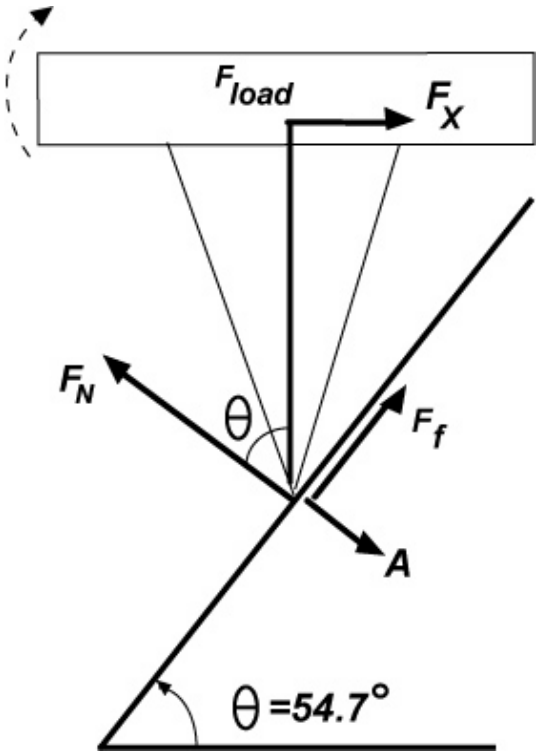

Figure 17: System of forces between the tip and the sloped surface, such that θ is always defined as the positive angle between the sloped surface and the horizontal plane

The equilibrium equations for this modified free body diagram are:

$$\sum F_{\parallel} = F_{Load} - (F_N - A)\cos\theta - F_f \sin\theta = 0$$

$$\sum F_{=} = F_X - (F_N - A)\sin\theta + F_f \cos\theta = 0$$

This new system of equations is problematic since we are left with 3 unknown variables (F_f, A, and F_N) in addition to the variable for which we are attempting to solve (F_x). However, if we assume that a linear relation between friction and the normal force holds at the nanoscale for the tip-sample interaction being considered, we can add the equation $F_f = \mu(F_N + A)$ as discussed in the Literature Review. If we measure the coefficient of friction and the adhesion force ahead of time, or if they are known from other sources, we can solve this system of equations for the lateral force (F_x) in terms of known quantities (See Appendix A) giving the following result:

$$F_x = \frac{F_{Load}(\sin\theta - \mu\cos\theta) - 2\mu A}{\cos\theta + \mu\sin\theta}$$

This equation uses F_X to represent the lateral forces acting on the cantilever, as expressed at the top of the beam, since F_X must equal the lateral forces acting on the tip for the principles of equilibrium to hold. Clearly, this expression differs quite substantially from Asay and Kim's result of $F_{Lateral} = F_{Load}\cos(\theta)\sin(\theta)$. In addition to having the additional terms involving μ and A, the general form is different even if we consider the case where μ=0 (and thus ignore friction and A, as Asay and Kim did). In this case, we have the result

$$F_x = \frac{F_{Load}\sin\theta}{\cos\theta}$$

This is clearly a significant difference from Asay and Kim's result, since we divide by cosθ instead of multiplying by it. This difference gives rise to substantially different behavior, as seen in Figure 18. There are several regions of particular interest in the adapted equation. First, consider the region as θ→0. In this region, the lateral force actually becomes negative, implying the force is actually in the opposite direction. However, it is important to recognize that this equation uses the assumption that $F_f = \mu(F_N + A)$, when in reality $F_f \le \mu(F_N + A)$ since we are only considering static friction. As such, if we use the inequality and assume that as θ→0, F_f→0, then the lateral force will never be negative, and will, indeed, approach zero as well.

The other region of interest is that when considering large angles, the modified equation presented does not go to zero as Asay and Kim's does. However, it is important to remember that the modified equation only holds true for angled surfaces, not vertical ones (i.e. for θ≠90°). However, for slopes leading up to the vertical the equation will hold, and implies that the lateral force needed to prevent slipping will increase as the slope increases.

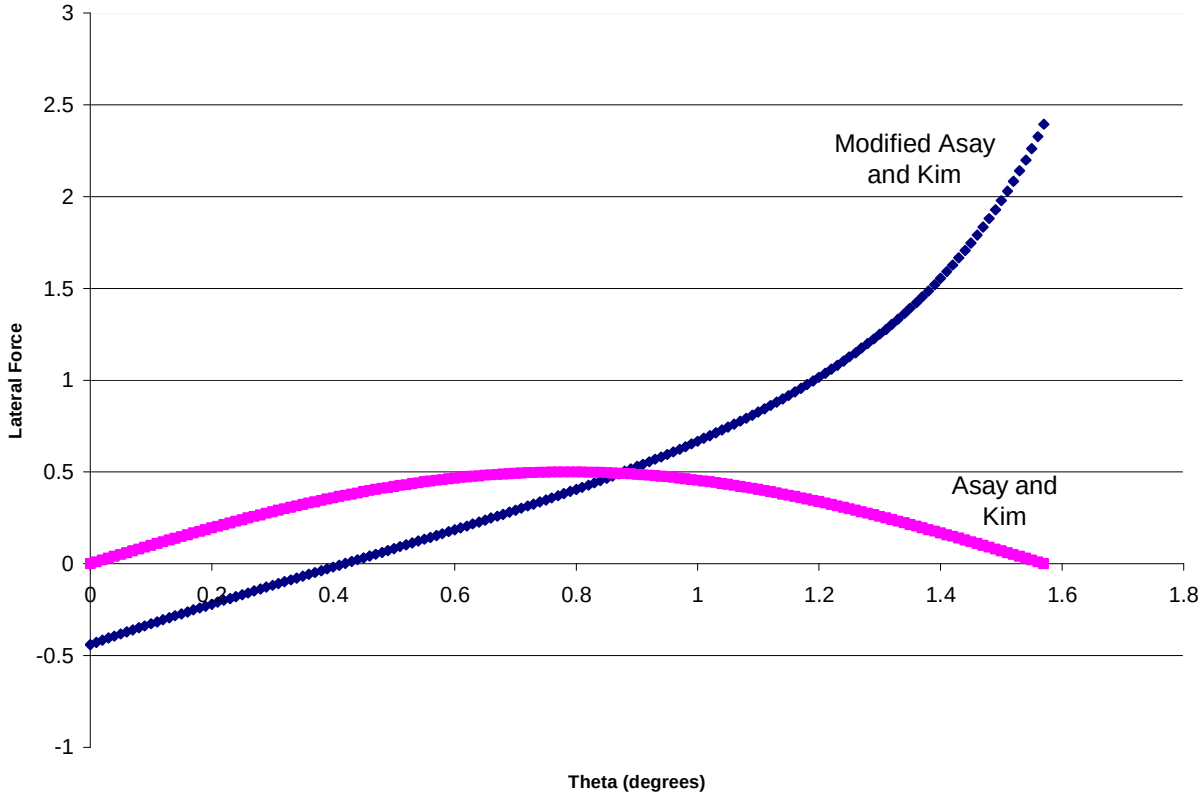

Figure 18: Functional difference between Asay and Kim's original equation and the modified equation for $\mu = .4$ and $A = .02$

Fortunately, the fundamental difference between these equations for the magnitude of the lateral force provides us with an approach to verify which equation correctly models the interaction. Specifically, we can see in Figure 18 the difference between the two equations: that they give different results for larger angles. As such, by performing the force-balance method on samples with widely varying angles, we can compare the results obtained from Asay and Kim's equation, and our modified equation. Since the lateral calibration factor is an inherent property of the cantilever being used, it should remain constant no matter what angle of incline the sample surface is. Because of the functional difference between the two equations, only one of them can correctly satisfy this requirement, and thus we can verify which (if either) equation is correct.

As our modifications on Asay and Kim's method depend directly upon the value of the friction coefficient μ, we must be careful to test whether a linear relationship exists between the silicon tip and the surface. While we assume that Coulomb-Amonton's Law holds true in our derivation, it is only necessary that a single surface be found with a linear friction relationship in order to calibrate the cantilever. To do this, lateral force scans were taken over silicon, graphite and mica samples while varying the normal force applied to the surface. Although the lateral data are uncalibrated, it gives us a relationship between the force on the surface and lateral signal to the photodetector. Figure 19 gives an idea of the possibilities for the frictional relationship, including the effects of adhesion and possible non-linear tip-surface relationships.

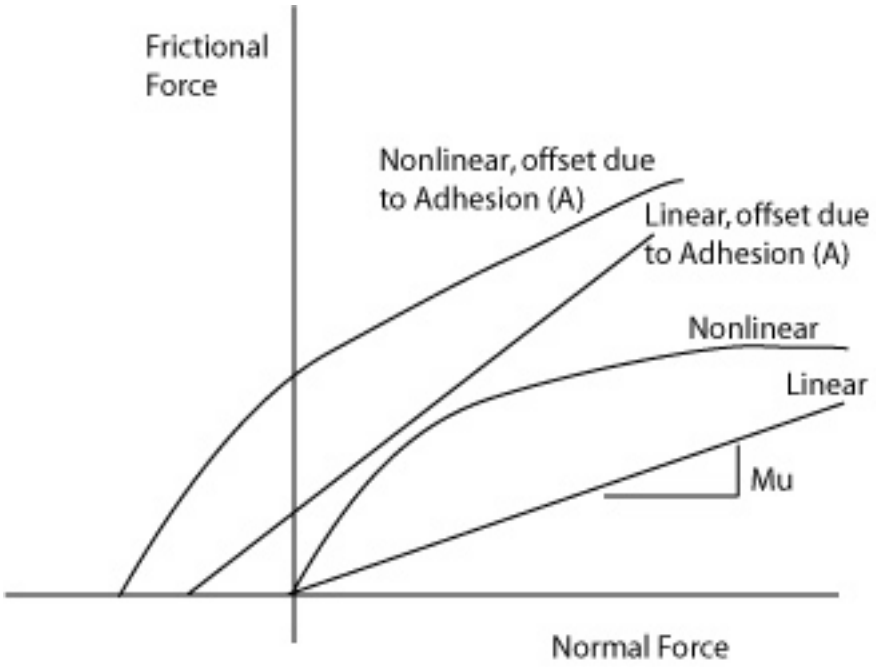

Figure 19: The different approximations for the relation between friction and normal force

It is also necessary to accurately measure the normal force applied to the surface by the cantilever. In Asay and Kim's paper, they use cantilevers that have been pre-calibrated by the manufacturer using the Sader method. In our experiment, we calibrate each cantilever using the wearless thermal method published by Burnham et al [9,16]. This allows us to accurately

measure the spring constant of the each cantilever to 10 % accuracy instead of limiting ourselves to high-cost pre-calibrated cantilevers or to the highly inaccurate spring constants supplied by the manufacturer for most cantilevers.

To thoroughly investigate the accuracies of these methods, it is necessary to compare them to an accepted method of calibration. As Asay and Kim's method attempts to reproduce calibration factors of high accuracy without the wear on the tip, it is crucial to compare these results with a method of known accuracy, such as Ogletree and Carpick slope-scanning method [10]. To complement the comparison of angular dependence of our modified method to Asay and Kim, we will compare the lateral calibration factors produced by each method with the Ogletree and Carpick method.

This step was overlooked in the paper published by Asay and Kim. In their testing and validation, they calculated a value for μ on their silicon sample, and argued that it fell within the accepted range for the coefficient of friction on silicon. While they were correct, the accepted range varies from as little as μ =0.02 to as high as μ=0.77 (MEMSnet.com, verify/cite specific studies). This makes measurements of μ a very poor yardstick for the validation of methods of calibration.

As all three methods require a sloped surface, a single calibration grating of known slopes may be used, provided it produces a linear frictional relationship and that μ has been measured. All three methods are reproduced on the Autoprobe M5 AFM systems using the X-Y trace mode. The tip is placed on a slope of interest, be it upwards, downwards, or a flat plateau, prior to engaging the X-Y Trace mode. To take lateral force curves, as prescribed in Asay and Kim's method as well as in our modified version, the X-Y trace mode is used to show the response in the lateral force signal proportional to the Z Detector motion. When the tip is in

contact with the surface, this relationship is linear. When out of contact, there is no lateral force component, and hence the graph is flat. Data are collected at a set normal force across multiple slopes.

The use of Ogletree, Carpick and Salmeron's method [10] to compare lateral calibration values requires a slightly different experimental approach. The tip is still placed on the slope of interest, but care must be taken, as this method requires scanning across a portion of the surface. The X-Y Trace mode is then engaged to show the relationship between lateral motion of the scan head (X-Drive) and the lateral force signal. These data must also be collected for differing slopes, but it must also vary in the normal force applied to the surface. This range of data can then be used to characterize the frictional response in the system.

By critically reviewing the force-balance approach presented by Asay and Kim, we have found a number of inaccuracies. This led to a closer look and to a reworked system of equations to represent the system, which in the end developed into an independent method for obtaining lateral calibration values. This provides us with the tools necessary to rigorously analyze the validity of the original method proposed by Asay and Kim, both experimentally and mathematically.

4 Experimental Approach

In the process of collecting data to support our modified force-balance method, it was necessary to establish the values of a number of constants and relationships within the system prior to data collection. These allowed us to look at the more complete picture and eliminate any doubt as to assumptions made in our model.

4.1. Linearity of Friction

In order to test our proposed calibration method, it was necessary to establish the validity of the assumptions incorporated in our model. The first of these was to look at the linearity of friction in our experimental system, as the assumption that $F_f = \mu(F_N + A)$ was integral to the construction of our force balance equations. This was done using the image analysis of signal images.

As our original samples had mica surfaces, our investigation of the linearity of friction was done on a flat, freshly cleaved mica sample. The specifics of the cantilever used were not important in this case, as we only needed to establish linearity, not a specific functional relationship. In this case, we used one of the unmarked previously used cantilevers, so specifications were unknown. In order to test for linearity, we took a very direct approach. It is simple to adjust the normal force applied by the cantilever to the surface by increasing or decreasing the set point voltage applied to the drive piezo. We then collected the lateral force data, or the amplified C-D signal off the photodetector, across a 5μm scan of the mica surface. This lateral signal is uncalibrated and it is recorded as voltage from the detector, but this is equally useful in our measurements. As the lateral calibration is a linear function, it would not affect the linearity of our data.

Scans were taken at six different set point values, ranging from -1 to -6 volts. The topographic representation of the data was primarily flat, but for a number of scans there was a sizable bump-type artifact that also appeared in the topographic signal. To obtain an average value for the kinetic frictional force observed with a given normal force applied by the cantilever, we used data analysis software to find the average height within the image, excluding the location of the bump-artifact on the surface. This average was then plotted as the dependent variable against the set point voltage used to examine the linearity of the relationship.

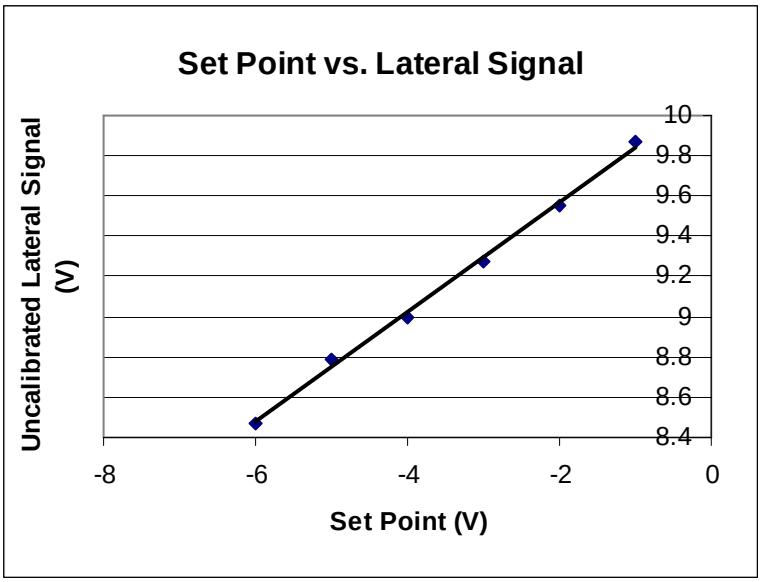

Figure 20: Analysis of the linearity of frictional force on mica for nano-scale measurements

As seen in Figure 20, we observed a highly linear relationship, with a correlation factor of R^2=0.9978. The value of μ cannot be determined from this plot, as the frictional force is in arbitrary units, but it is known that as the slope of this plot is constant, that μ must also be constant. This allows us to safely make use to the assumption that $F_f = \mu(F_N + A)$ in our rederivation of the force balance equations.

4.2. Calibration of Cantilever Normal Response

All models used in lateral force calibration require precise knowledge of the normal force within the system. On mass-produced AFM cantilevers, the normal force constant is often reported to +/-50% accuracy. As this is far from precise, a number of methods were employed to check the response of a given cantilever against the reported factory value, and also to determine the actual normal force applied more precisely.

4.2.1 Resonance Calibration Method

In our initial labwork, we had not determined the precise model of cantilever necessary for our force-balance measurements, so we used an assortment of previously used cantilevers. However, these cantilevers were unlabeled, so it was not possible to reference the manufacturer's quoted values for normal response.

To obtain a rough estimate of the normal spring constant of the cantilever, we employed a resonance relationship. This method, an improvement over the basic methods which rely only on the dimensions of cantilever, uses the resonance frequency of the cantilever in air along with dimensions to approximate the normal spring constant. Because our cantilevers were unlabeled, this posed a problem as the measurements were also unknown. Since a limited number of styles of rectangular cantilevers are used in our lab, it was possible to correlate the aspect ratio of a cantilever to known measurements to narrow down the style of the cantilever.

This was completed by placing the chip-mounted cantilever under an optical microscope, equipped with a relative measurement scale on the objective. This allowed us to find the ratio of cantilever length to width, and compare this to possible cantilevers. As this was often difficult, we calibrated the reference scale at minimum magnification against a cantilever of known style. We were then able to directly approximate the length and width of the cantilever. While we

could not measure thickness, this varied far less between rectangular cantilevers, usually 2um or 3um. It was also possible with known length and width measurements to look up the thickness of the cantilever.

The resonance frequency of the cantilever was found using the non-contact measurement (NCM) functionality of the AFM. By mounting the cantilever onto the scan head and activating the NCM mode, we were able to use the piezo drive in shaker mode to excite vibrations in the cantilever and find the peak in the resonant response. With the dimensions and resonant frequency of the cantilever, we used Equation A to approximate the normal constant for the cantilever.

Equation A: $k_c = 2w(\pi * l * \nu_0)^3(\rho^3 / E)^{1/2}$

$\rho=2.330*10^3$ kg/m^3

$\nu=1.1*10^{11}$ N/m^2

While somewhat effective for unmarked cantilevers, the number of assumptions and approximations made in this method make it highly unreliable, with accuracy on the same order as the manufacturer's published values. The pre-used cantilevers provided useful for initial labwork, but with the high inaccuracy in the normal calibration made them useless for data collection.

4.2.2 Thermal Calibration Method

Since a more precise knowledge of normal forces in our system was needed, we discarded the resonance method. We employed the methodology developed by Erik Thoreson and Dr. Nancy Burnham in the WPI AFM Lab to use thermal characteristics of the cantilever to find the normal spring constant. This method is much more accurate, certified to +/- 10% off NIST benchmarks. This method is described in detail in an appendix of Erik Thoreson's doctoral dissertation [16].

For this method, the AFM needed to be interfaced with a separate data collection computer. This was set up on the Alpha machine in the lab, while a majority of our early research was completed on the Beta machine. Because of this, the cantilever needed to be remounted between calibration and when data for the force-balance system could be taken. However, the use of this method did assist to verify the spring constants of newly purchased cantilevers, which were used for the rest of the experiment.

4.3. Initial Lateral Calibration via Accepted Methodology

One of the oversights made in the original paper by Asay and Kim was the omission of any comparison to accepted methods. In order to access the validity of the original and of our modified force balance system, we wanted to obtain a baseline value for the lateral calibration factor, using the widely accepted method published by Ogletree, Carpick and Salmeron. This would, in theory, provide us a "correct" value off which to base our comparisons.

The method proposed by Ogletree et al, described in the Literature Review section here, requires that the normal force on the surface be varied during the scan of the surface. In their publication, they suggest incrementing the normal force applied during each individual line scan, of the 256 scanlines which constitute an image. The Autoprobe M5 AFM used for this research, had no existing support for this method. Because of this, we could only manually bracket the set point during the scan. This manual restriction translated to a practical limit of about ten steps per scan, which was far less than was needed to accurately determine the lateral calibration factor.

It was recognized that it would be possible to overcome these limitations in the future by developing a method for computer control of the set point increases, or by development of a system using the X-Y trace instead of successive scan lines. However, as this calibration method was not the central focus of our research, we shifted the project focus to the force-balance

method, and planned to return when we needed to compare and validate lateral calibration values found using these newer methods.

4.4. Preliminary Lateral Force Curves

4.4.1 Milled Samples

After doing the necessary background work, we moved on to work on collecting the necessary Lateral Force Distance curves. Our original intent was to take these curves on several milled samples of known slope (ranging from 12º to 20º) with smooth mica surfaces attached. Using these milled samples would be advantageous due to the ease of using a sample with a single slope, and the mica surface was one on which we had already verified a linear friction relationship, and could easily perform additional tests as needed. Unfortunately, the size of the sloped samples prevented us from taking force distance curves, since doing so would result in the cantilever holder striking the sample before the cantilever tip would, as seen below.

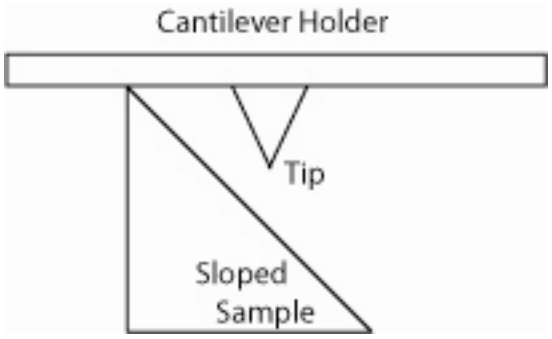

Figure 21: Problem arising from using a large sloped-surface sample

To avoid this problem, the tip could be lined up with the very top of the slope, but this presented additional problems. First, the region in which the tip could properly reach the sample was very small, making such an alignment extremely difficult. In addition, the edge of the mica was not strongly attached to the milled sample in that region, such that it could move slightly when pressed, and it was not exactly the same angle as the milled sample, both of which would

be problematic when attempting to gather the necessary data. Because of these problems, the milled samples were abandoned, and alternate sources of sloped surfaces were used.

4.4.2 Calibration Gratings

To avoid the problems caused by the use of macroscopic sloped surfaces, we began using calibration gratings, specifically the TGG01 and TGF11 gratings from MikroMasch.

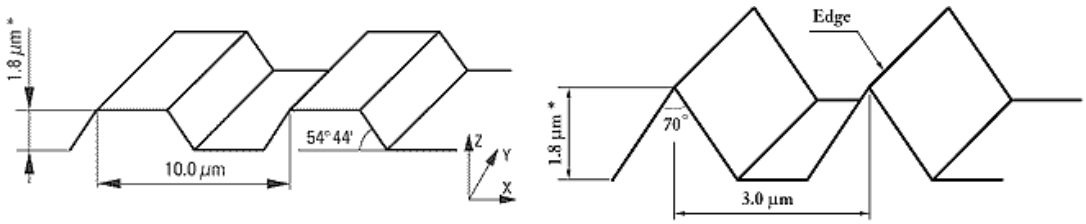

Figure 22: TGF11 (left) and TGG01 (right) gratings. Diagrams from MikroMasch (www.spmtips.com)

Since the height of these slopes were shorter than the cantilever tip, there were no problems attaining proper tip-sample contact to take the force curves. Additionally, each sample could provide us with 3 different slopes on which to take data (0º, +55º, and -55º) without the need to tilt the overall sample. To distinguish between these three regions, the terminology in Figure 23 will be used for the remainder of this paper.

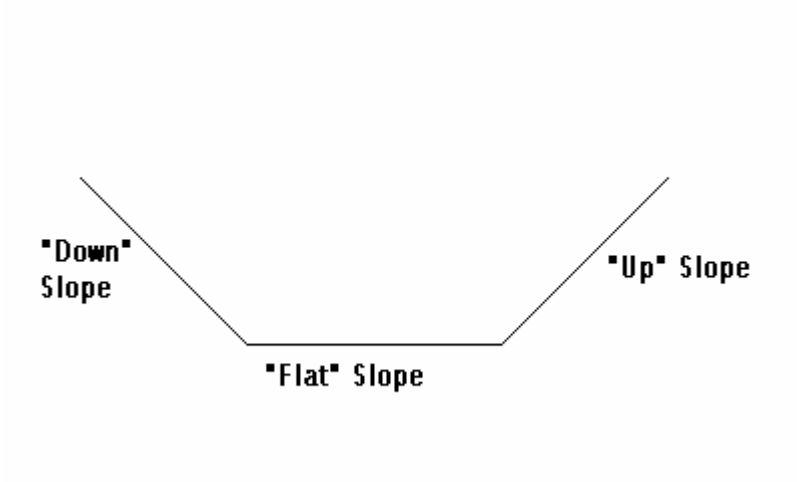

Figure 23: Slope Terminology

Using the method described in Appendix B, we began taking Lateral Force Curves on all three slopes of each calibration grating.

Unfortunately, we ran into several problems with the data collected in this manner. The primary problem was that the force curves we obtained were extremely noisy, to the point that it was difficult to see any correspondence between our data and the distinctly linear graphs acquired by Asay and Kim. Samples of the curves obtained on all three slopes (up, down, and flat) are given in Figures 24-26.

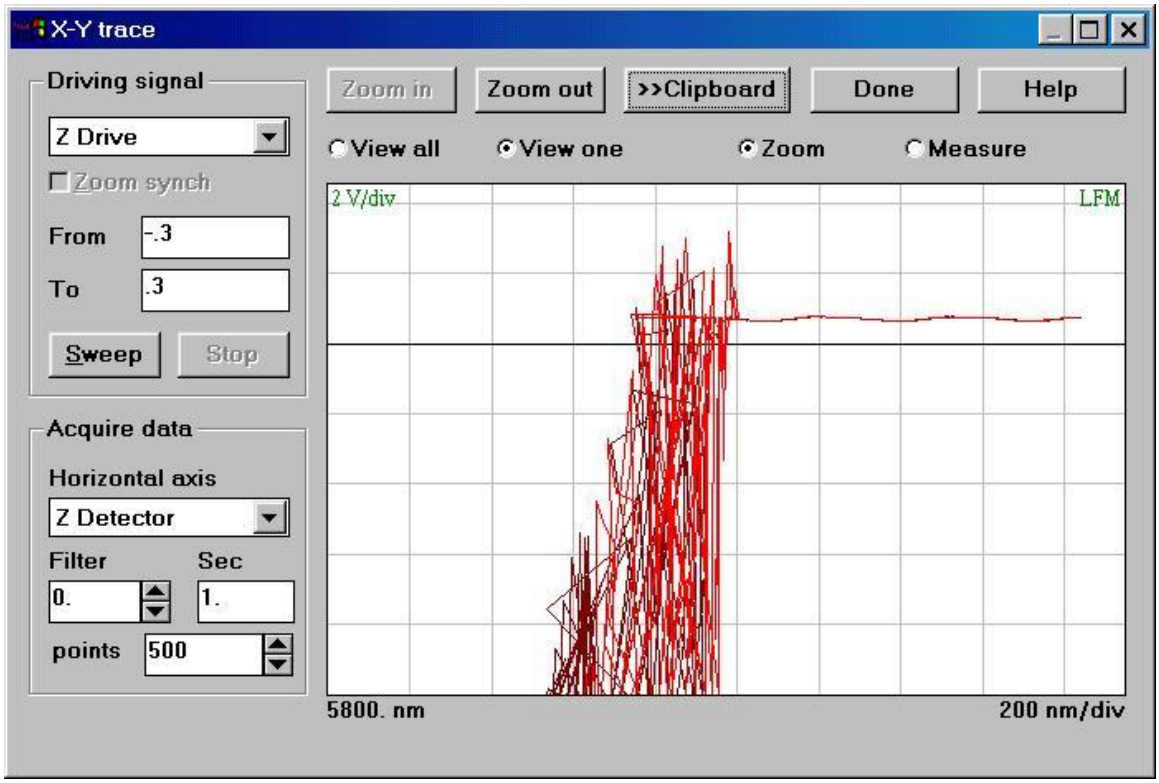

Figure 24: Lateral Force Curve taken on the Down Slope

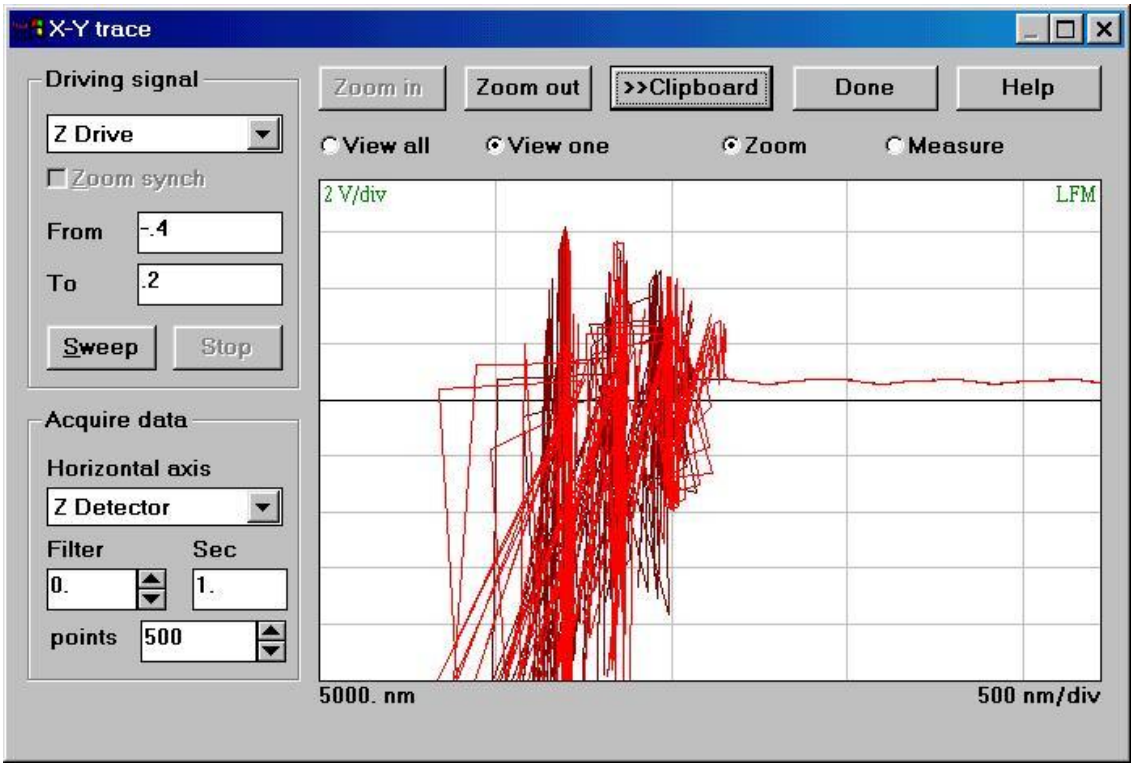

Figure 25: Lateral Force Curve taken on the Flat Slope

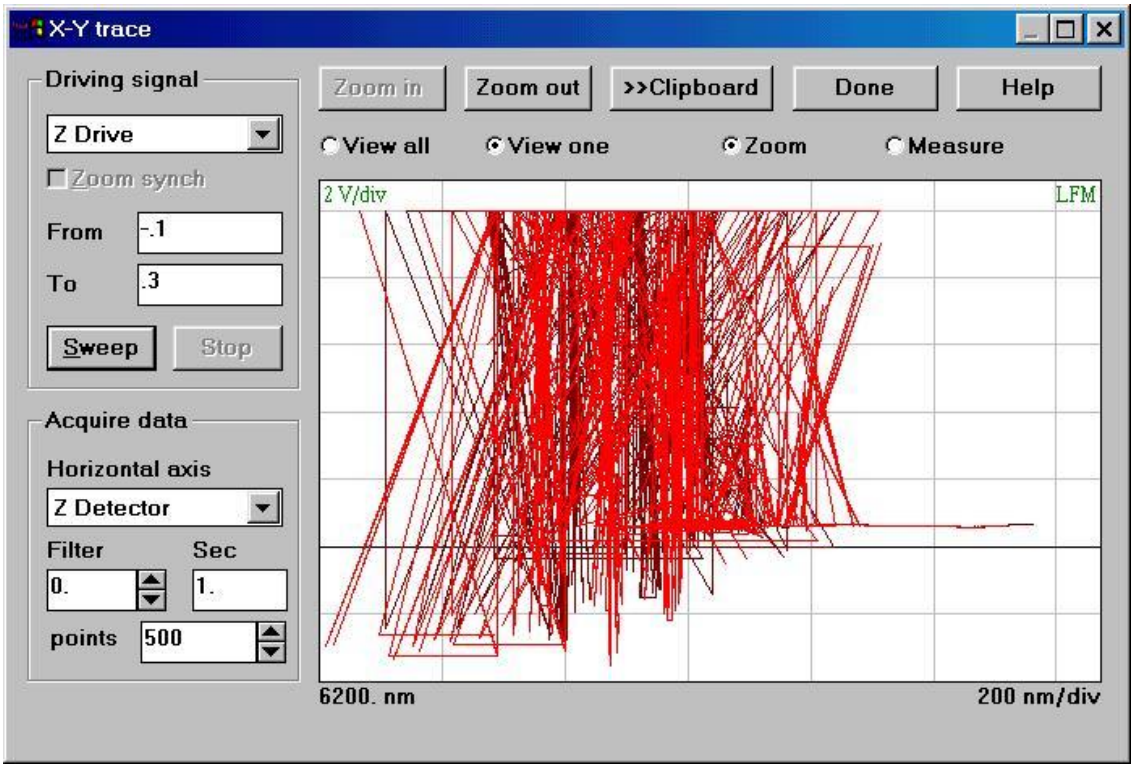

Figure 26: Lateral Force Curve taken on the Up Slope

In an attempt to more effectively produce graphs such as those presented by Asay and Kim, we try varying the Filter over the entire range of accepted values, with no noticeable effect. By taking the curves over a longer time period, there would frequently be fewer lines visible, but otherwise would have no substantial difference (nor would changing the number of data points collected).

Despite the sizeable noise, we attempted to save the data so as to import it into another program that would allow additional data analysis. However, when attempting to copy and paste the data (the only way to save the specific data) into Microsoft Wordpad, we were invariably presented with an error message followed by the program crashing prior to saving, thus preventing any data analysis using additional programs. Since the only quantitative analysis that could be done with the types of graphs attained would be estimate the slope by eye (which is completely infeasible for graphs such as we obtained), we were forced to temporarily abandon

this method in favor of one with more reliable results. This method was extended upon later in the project (see Section 4.6).

4.5. Normal Force Curves

In hopes of obtaining less noisy data, as well as avoiding the problems with saving data from lateral force curves, we decided to attempt to gather equivalent graphs, but for the normal force, rather than the lateral force. By rotating the sloped sample 90º, the force calculated in Appendix A would actually be applied to the cantilever as a normal, not lateral force. However, since the calculations performed were independent of the direction of the cantilever beam, the hope was that we would be able to gather data which, while not useful for lateral calibration, could be used to verify the accuracy of the equation presented by Asay and Kim, as well as our modification to it.

Since the sloped surfaces were rotated 90º, the milled samples could now be used without any risk of the cantilever holder striking the sample, so they were used for the simplicity of a single slope rather than the 3 slopes found on the calibration gratings. The data collected from this were simple fd-curves, and there were no problems obtaining them, nor saving them. However, the results were not usable for this project, since the force obtained was a combination of the force calculated in Appendix A and the normal force cause by the cantilever pressing down against a surface, and we were unable to develop a way in which to isolate the data of one force from the other.

4.6. Further Lateral Force Curves

With the inability to use data from the normal force, we returned to taking lateral force curves. While we were unable to get data significantly improved over that in Figures 24-26, we determined that the specific data points could be saved by the rather convoluted process of copying and pasting it into Notepad and saving, while ignoring the error messages which were given, and then by opening the saved file in Wordpad. Upon discovering this, we were able to export the data to Microsoft Excel to perform proper data analysis, which began to yield much more interesting results (described in the following section).

Because we were then able to perform effective data analysis on the lateral force curves, we spent more time taking data over as many different angles as possible, since our hope was to verify whether our method (or that proposed by Asay and Kim) provides an accurate lateral calibration independent of the angle of the sample used. The calibration gratings each had 3 slopes on which we could take data, and to consider additional slopes, we tilted the overall sample. Several methods were attempted, the most effective of which was to simply place the calibration grating such that only one edge was on the raised sample holder, and the other was on the surface of the stage. By unscrewing the sample holder various amounts, we were able to tilt the grating up to ~10º, which was the maximum angle that could safely be used without risk of the cantilever holder striking the tilted sample, just as was the case with the milled samples (And even angles <10º required moving the grating to the edge of the magnetic mount on which it was attached). While it was impractical to use this method of tilting to obtain a specific angle, by taking a scan of the sample, and performing a line measure on the topography signal, we were accurately able to determine the angle after the fact, which was all that would be needed for the

method (which ideally should work for *any* angle, and thus there is no need for selecting a particular one ahead of time).

5 Data Analysis

5.1 LFM vs. Z Detector

The main relationship we needed to consider was the lateral signal as a function of the Z Detector, since the slope of this graph would, in theory, give us the information we needed to test Asay and Kim's equations as well as our own. Because we are looking for the slope of the function, we expect the behavior to be linear when in contact with the sample, and flat when out of contact (for large Z-detector signals). As seen in Figure 27, the out of contact behavior is horizontal with the lateral signal at approximately 0 Volts as expected, but the in region in contact with the sample, the signal is most assuredly non-linear.

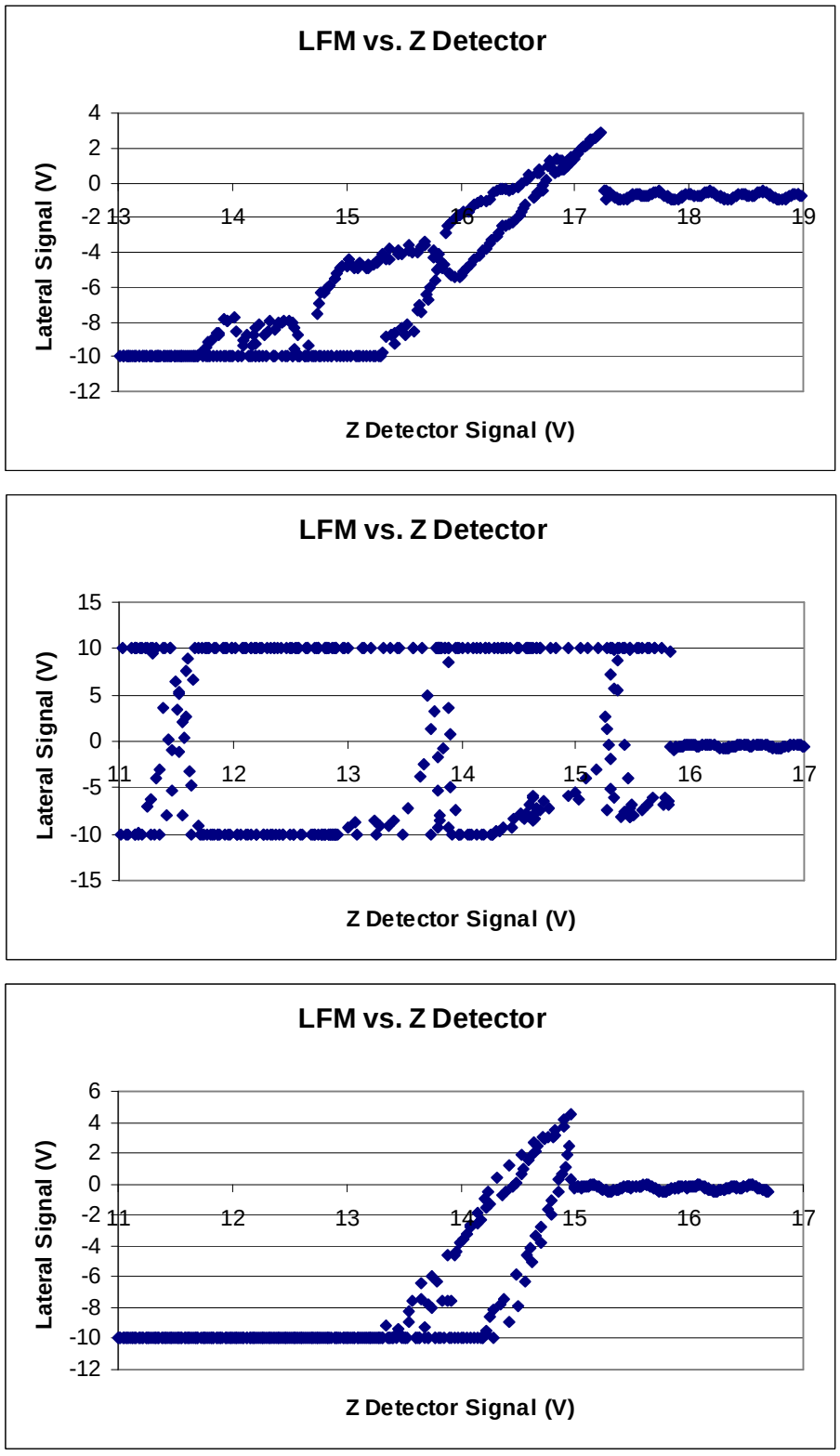

Figure 27: Lateral Signal vs. Z Detector on (a) a flat silicon sample (b) a sloped silicon sample (upslope) (c) A sloped silicon sample (downslope)

As these results are substantially nonlinear, there is no way to use them in the calibration method we were attempting to verify. We then began looking into the behavior of the system to determine why the results were sufficiently different from our assumptions.

5.2 Z Detector and Lateral Signal Behavior

To explain the behavior, we began looking at the Z Detector signal. We expected the Z Detector to behavior linearly with time, since it is the absolute position of the scanhead during the force-distance curve. While this expectation was confirmed by an employee at Technical Support for Veeco Metrology Instruments, our data did not support it. As can be seen in Figure 28, the Z Detector has an overall linear pattern, but there are regions in which there are significant oscillations.

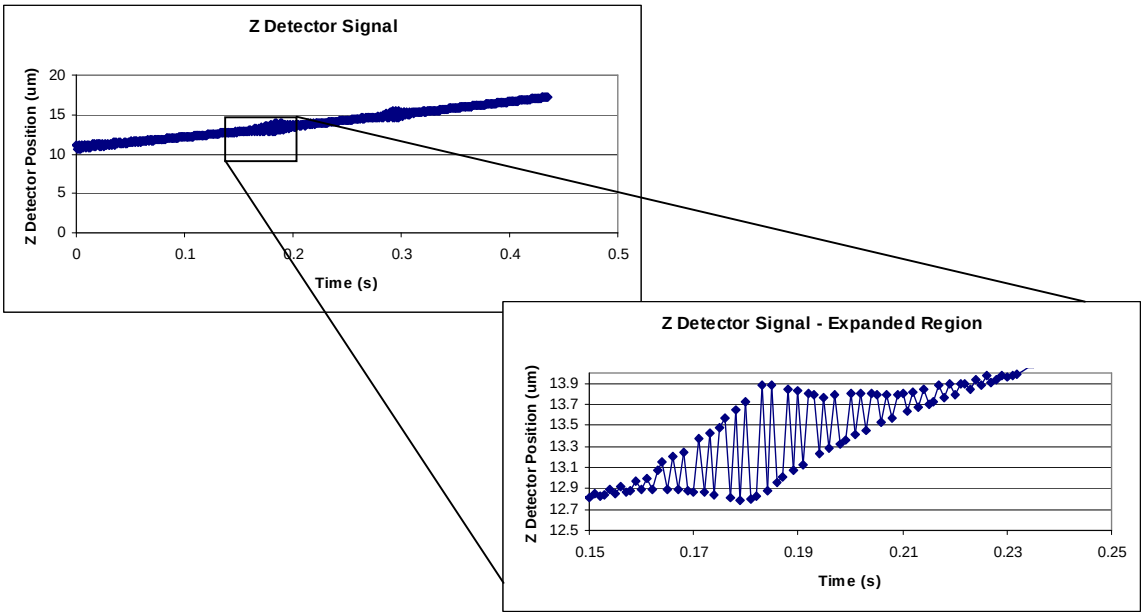

Figure 28: Z Detector vs. Time with focus on oscillatory behavior

These oscillations were observed on numerous occasions, implying that they may not simply be random noise. To better view them, we used Microsoft Excel's Trendline function to find the equation for the line formed by the overall linear behavior of the curve, and subtracted

this out. By doing this we can see the deviation of the Z Detector signal from the expected linear behavior. We can them compare these deviations with the behavior of the lateral signal, as in Figure 29.

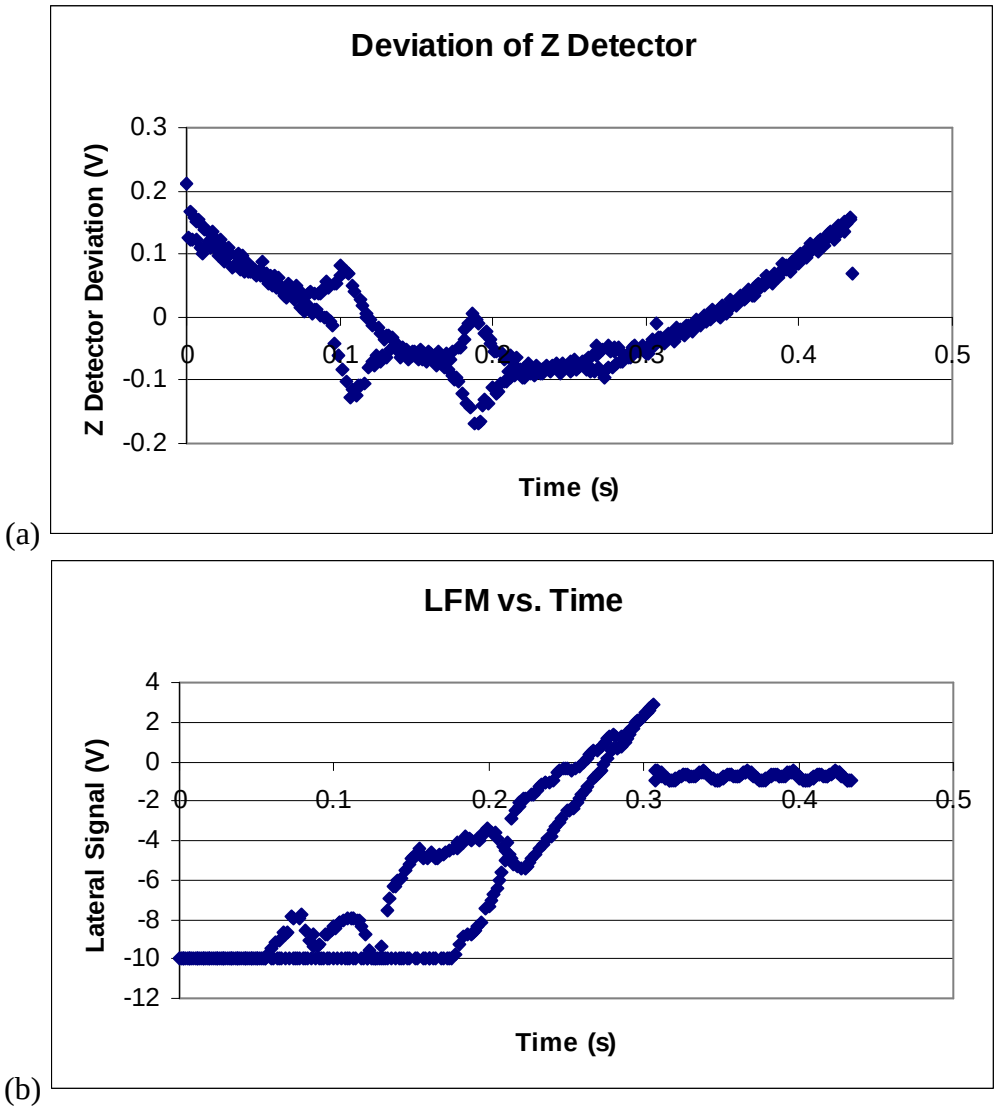

Figure 29: (a) Z Detector Deviation vs. Time and (b) Lateral Signal vs. Time on a flat surface.

The data obtained in Figure 29 are significant for several reasons. First, we can see that the LFM versus Time graph does not seem to be noisy, but rather it follows two distinct paths. When compared with the LFM versus Z Detector graph (Figure 27a), we can see that the lateral signal is much smoother when plotted versus time than it is when plotted versus the Z Detector

Signal, implying that a significant portion of the noise in the lateral signal seen in Figure 27a is actually due to the oscillations in the Z Detector.

Since at least some of the noise is due to the behavior of the Z Drive, there is the possibility that the overall behavior of the lateral signal might be related to the Z Drive as well. To better consider this possibility, additional Z Detector Deviation curves were plotted, along with their associated LFM versus Time curves (Figures 30 & 31).

(a)

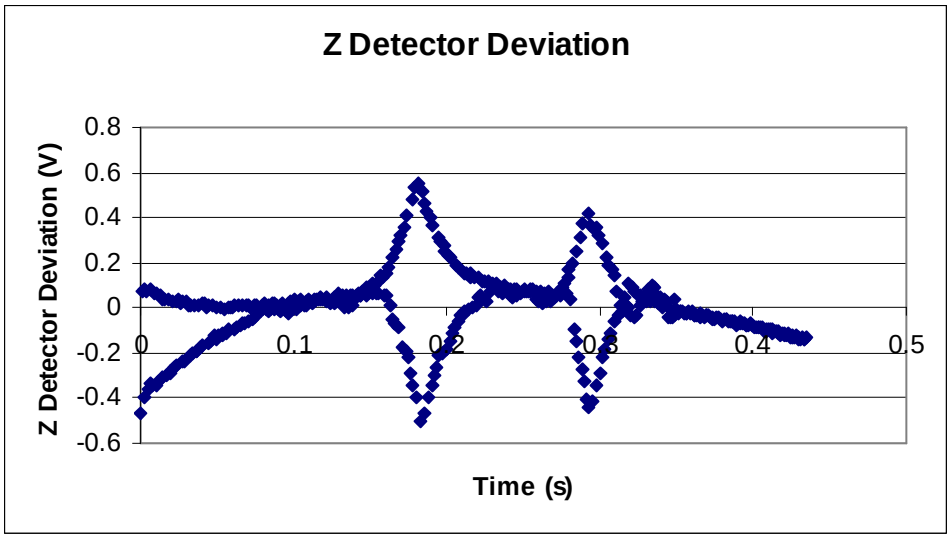

(b)

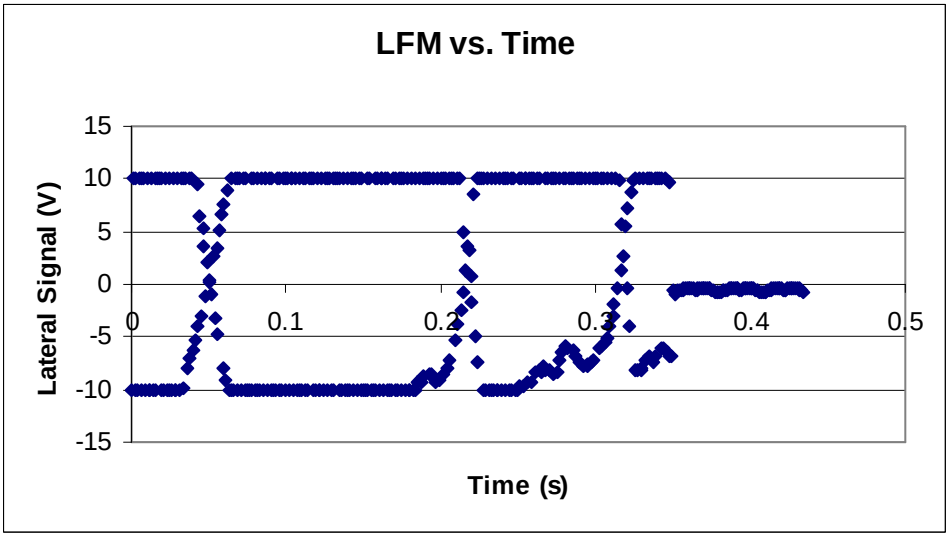

Figure 30: (a) Z Detector Deviation and (b) Lateral signal vs. Time curves for an upward sloped silicon surface

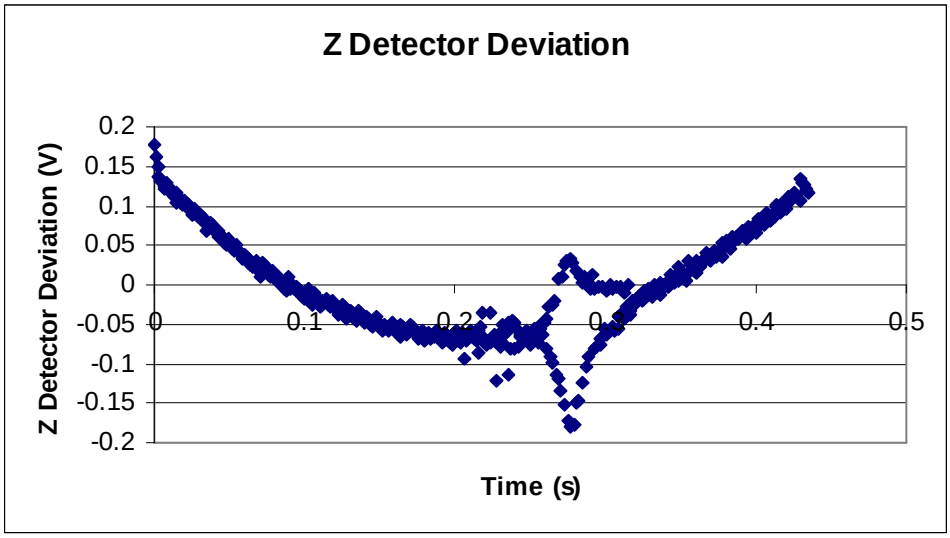

(a)

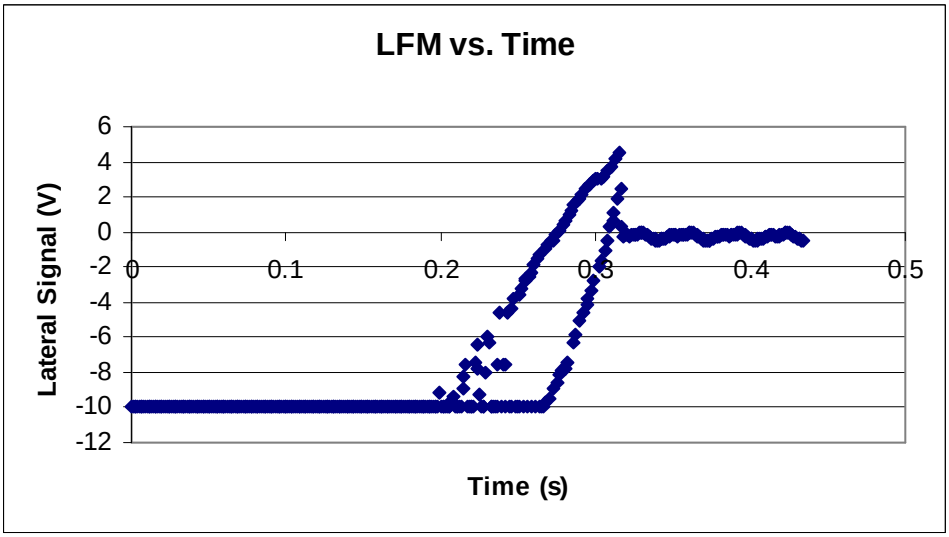

(b)

Figure 31: (a) Z Detector Deviation and (b) Lateral signal vs. Time curves for a downward sloped silicon surface

By looking at the relationship between the Z Detector and LFM curves in Figures 30 & 31, we can see that there seems to be some correspondence between the deviations in the Z Detector and the behavior of the lateral signal. Specifically, each bump in the deviation seems to be consistent with the jumps between lines in the LFM signal, and this pattern continues in numerous other datasets collected over the course of the project. This correlation appears to be key to understanding the reason behind the lateral signal behavior.

5.3 Error Signal

While attempting to establish the source of the oscillations in the Z-Detector signal, we looked closely at the error signal output of the AFM. This signal is the difference in voltage between top and bottom portions of the photodetector signal. Where the oscillations in the LFM signal showed that the cantilever was twisting laterally, any oscillations in the error signal would indicate that the cantilever was also bending vertically while the force distance curve was taken. Figure 32 shows the normal oscillations increasing with the normal force while the tip was placed on the downward slope.

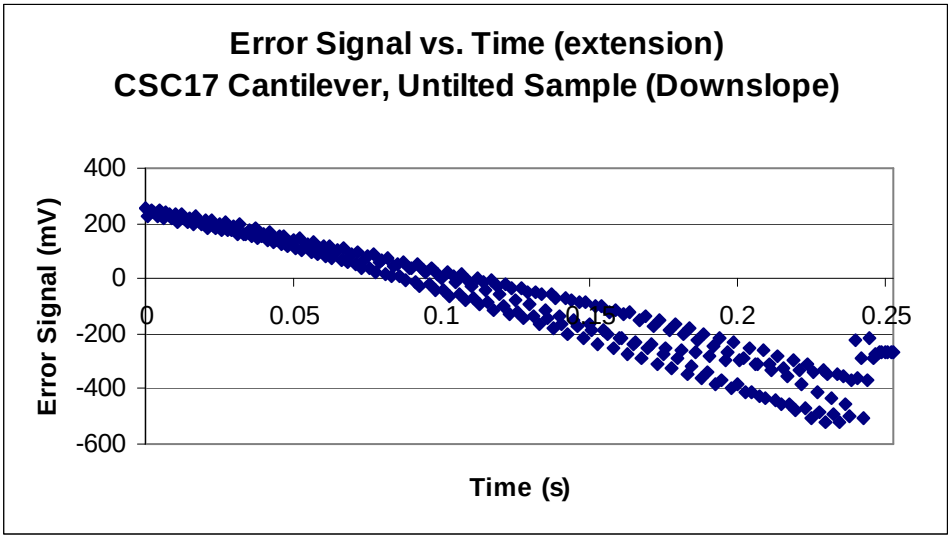

Figure 32: Error signal plotted versus time, showing increasing oscillations during the extension portion of the force-distance curve.

This pattern in the error signal varied for different angled surfaces. When we took data on the flat plane surface, the error signal versus time plot was very linear and showed no deviation. On the upslope, we noted a much larger oscillation of the error signal, and also a clearer pattern of events, mimicking the phenomenon we noted in the Z Detector. This is shown in Figure 33.

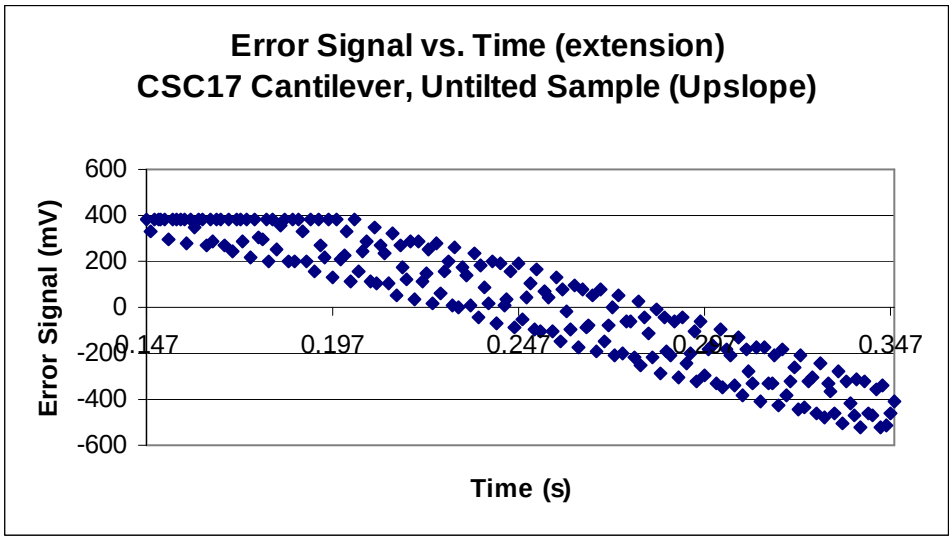

Figure 33: Error signal versus time on the upward slope, with much larger oscillations in the signal.

5.4 Possible Explanations

By looking at the error signal plots, it becomes apparent that this phenomenon is not isolated in one signal or dimension of cantilever motion. Because of this, there are a number of possible causes which must be considered.

5.4.1 Slip-stick interaction

One of the first hypotheses that came up was that of slip-stick interaction between the silicon tip of the cantilever and the silicon calibration grating. This idea is that irregularies in the surface interaction could cause the cantilever to become "stuck," which would increase the rotation of the cantilever until enough force is built up to force the tip to "slide." However, this hypothesis is still under investigation, and so is not sufficiently documented or understood for us to show any relation of our data to this hypothesis.

5.4.2 Instrument malfunction

Another natural explanation of this phenomenon is that of instrument malfunction. As the AFM systems used in this project have been through a fair amount of abuse, it is a fair assumption that there could be some sort of problem. If there was an issue in the drive piezo, this could explain the Z-Detector deviations observed. If the photodetector was malfunctioning, the signal collected by the computer could be flawed.

To test this explanation, we used two separate scanheads, from the Alpha and Beta machines, to collect data. The majority of our data were collected using the Beta scanhead on the Alpha system, but as shown in Figure 34, the Alpha scanhead on the Alpha system produces the same phenomenon.

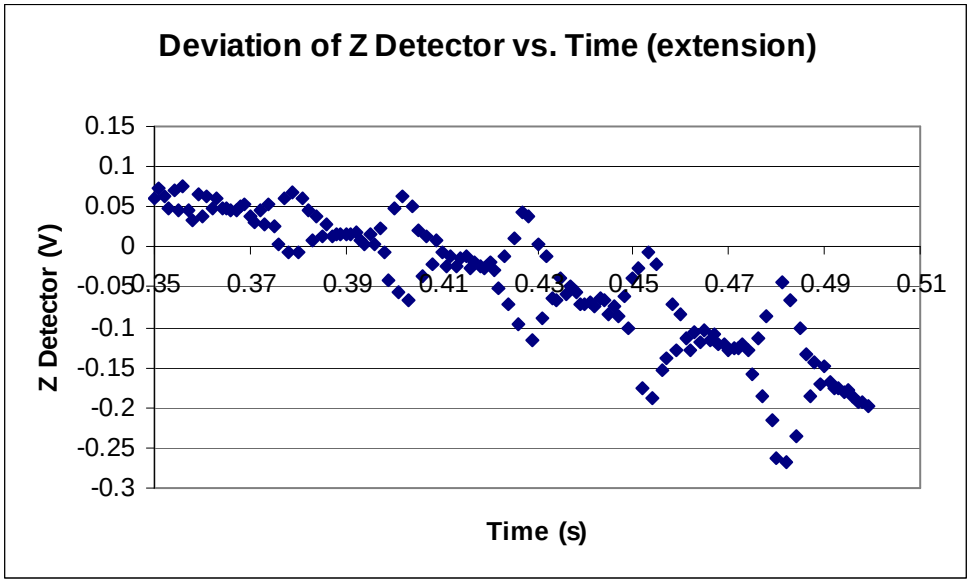

(a)

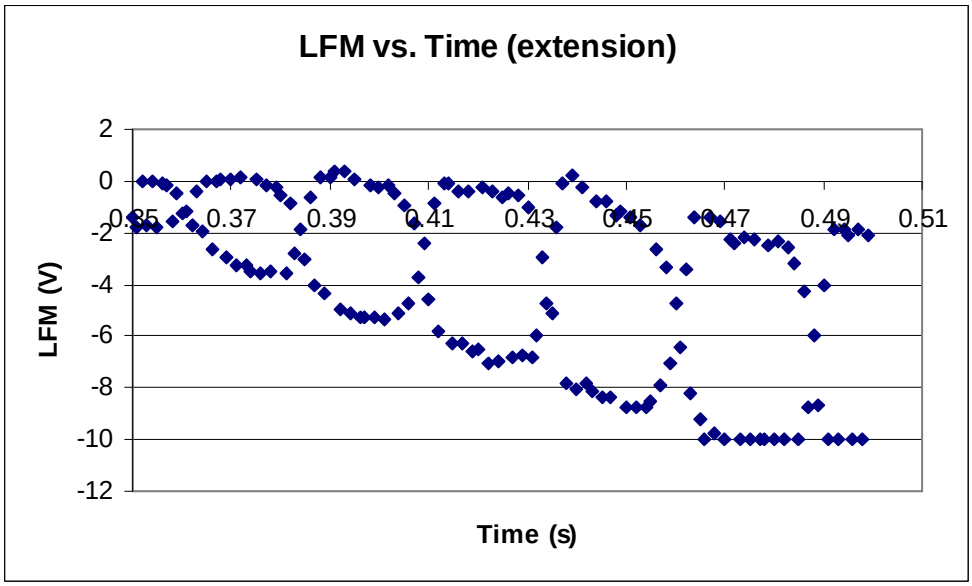

(b)

Figure 34: Data collected using Alpha scanhead demonstrate similar characteristics to that collected using the Beta scanhead.

These data were taken using the same style of cantilever on the same calibration grating as the majority of our data. This indicates that malfunction within the scan head is unlikely to be the cause of the observed phenomenon. While our final data all come from the Alpha machine, it is highly unlikely that the error is introduced by the Z-stepper motor, as the lateral force-

distance curve only requires motion in the scanhead. The Z-stepper motor on the Alpha machine has been shown to work well in our experiments, as well as others, showing no irregularities which would affect our data.

5.4.3 Fundamental instrument design

While we have tested for possible malfunctions in the instrumentation, it is impossible to rule out the theory that a problem in the instrument design of the Veeco Autoprobe M5 is causing the phenomenon we have observed. We are in communication with a Technical Support technician at Veeco to isolate possible sources of error.

As part of these discussions, the technician ran a similar experiment to ours, looking at lateral force signal versus Z-Detector position, and produced a graph very similar to that obtained by Asay and Kim. Since this was done on a similar machine, it suggests that it is either our experimental design or our calibrationsthat are the cause of the phenomenon, not the machine.

5.4.4 Other Sources of Error

There are many other possible sources of error which we have not yet discovered. Because the phenomenon is repeatable across different samples, sample angles and orientations, cantilevers (of different resiliency), and even different scanheads, the effect is far from random. Any source of error would have to be very regular and very repeatable, which takes weight away from environmental conditions, especially as our data were collected over a series of months.

6 Discussion of Project

6.1 Accomplishments

While this project did not succeed in the original goal of disproving the equations proposed by Asay and Kim [15] while verifying our own, it was a success in several other aspects. First, the theoretical work involved a thorough investigation of a proposed method, and a careful breakdown of the assumptions made by Asay and Kim, particularly those which were not explicitly stated (and thus has no supporting justification). This demonstrated the importance of clearly stating assumptions and making sure they are reasonable by noticing the radical difference between Asay and Kim's final equations and our modifications.

After analyzing their recently proposed method, we prepared a detailed critique, which included our proposed modification and accompanying derivations. This necessitated the development of an experimental procedure (described in Section 3: Methodology) which could be used to prove or disprove our assumptions and modifications. While the data collection was underway, we were required to constantly update our plans and modify the type of data being taken to account for the unexpected results we obtained. Additionally, substantial progress was made in methods of data analysis that could be used to extract usable data from seemingly random noise.

6.2 Significance of Project

This project has laid the groundwork for future research in lateral calibration. Given WPI's involvement in normal calibration [9,16], this course of study comes naturally. The discovery of the oscillatory behavior in the WPI AFM systems is of crucial importance to future research within any field in this lab. While the oscillations were very apparent in our data

collection, in other research the error could be more subtle while still causing defects in the results. This is an important phenomenon to explain and attempt to eliminate, and now that it has been discovered, this process can begin.

The work done on Asay and Kim's method is also of distinct significance. For the scientific community as a whole, the correction of flawed methodology within peer-reviewed journals is of high importance. It alerts those in the field to look more critically at current research, and to question common assumptions. In the same vein, industry has a clear need for a method of nondestructive calibration for lateral measurements. Our work outlined a method to validate the new methodology against accepted and commonly used methods.

6.3 Future Research

While our project made clear progress, there are many avenues upon which more work may be done. One such path that became very clear was the need to automate normal force increases mid-scan, such that the commonly used method of Ogleetree, Carpick and Salmeron [10] may be used on the Autoprobe M5 AFMs. This is largely a problem of application, but it would assist any future group working in lateral calibration, or anyone who needs a better understanding of forces applied at the AFM tip.

More closely tied to our project is the desire to achieve our working goal, to publish a review of Asay and Kim's work and to shed light on the assumptions and errors made in their paper. However, before this can be done the source of the oscillations in the AFM signal must be isolated such that data may be produced for the analyses of the conflicting methodologies. In this exploration, a better understanding of the surface interactions between tip and sample would be invaluable. Until this is done, it is difficult to know whether slip-stick phenomenon is indeed the source of our errors.

References

[1] Reitsma, M., Cain, R., Smith, D., Biggs, S., Page, N. “Lateral Force Microscopy: A Tool for Tribology.” GeoEng 2000 Conference, 2000

[2] Gnecco, E., Bennewitz, R., Gyalog, T., Meyer, E. "Friction experiments on the nanometre scale." *Journal of Physics: Condensed Matter* **13** (2001) R619-R642.

[3] Falvo, M., Superfine, R. “Mechanics and friction at the nanometer scale.” *Journal of Nanoparticle Research* **2** (2000) 237-248

[4] Carpick, R.W., Salmeron, M. "Scratching the Surface: Fundamental Investigations of Tribology with Atomic Force Microscopy." *Chemical Review* **97** (1997) 1163-1194.

[5] Beake, B., Legget, G., Shipway, P. “Frictional, Adhesive and Mechanical Properties of Polyester Films Probed by scanning Force Microscopy.” *Surface and Interface Analysis* **27** (1999) 1084-1091

[6] Mate, C.W., McClelland, G.M., Erlandsson, R., Chiang, S. "Atomic-Scale Friction of a Tungsten Tip on a Graphite Surface." *Physical Review Letters* **59** (1987) 1942-1945.

[7] Ruan, J., Bhushan, B. "Atomic-Scale Friction Measurements Using Friction Force Microscopy: Part I - General Principle and New Measurement Techniques*." ASME Journal of Tribology* **116** (1994) 378-388.

[8] Sader, J.E., Chon, J.W.M, Mulvaney, P. "Calibration of rectangular atomic force microscope cantilevers." *Review of Scientific Instruments* **70** (1999) 3967-3969.

[9] Matei, G.A., Thoreson, E.J., Pratt, J.R., Newell, D.B., Burnham, N.A. “Precision and accuracy of thermal calibration of atomic force microscope cantilevers.” *Review of Scientific Instruments* **77** (2006) 083703-1 - 083703-6.

[10] Ogletree, D.F., Carpick, R.W., Salmeron, M. "Calibration of frictional forces in atomic force microscopy." *Review of Scientific Instruments* **67** (1996) 3298-3306

[11] Varenberg, M., Etsion, I., Halperin., G. "An improved wedge calibration method for lateral force in atomic force microscopy." *Review of Scientific Instruments* **74** (2003) 3362-3367.

[12] Tocha, E., Schönherr, H., Vansco, C.J. "Quantitative Nanotribology by AFM: A Novel Universal Calibration Platform." *Langmuir* **22** (2006) 2340-2350.

[13] Reinstädler, M., Rabe, U., Scherer, V., Hartmann, U., Goldade, A., Bhushan, B., Arnold, W. "On the nanoscale measurement of friction using atomic-force microscope cantilever torsional resistance." *Applied Physics Letters* **82** (2003) 2604-2606.

[14] Bilas, P., Romana, L., Kraus, B., Bercion, Y., Mansot, J.L. "Quantitative characterization of friction coefficient using lateral force microscope in the wearless regime." *Review of Scientific Instruments* 75 (2004) 415-421.

[15] Asay, D.B., Kim, S.H. "Direct force balance method for atomic force microscopy lateral force calibration." *Review of Scientific Instruments* **77** (2006) 043903-1 - 043903-9.

[16] Thoreson, E.J. "From nanoscale to macroscale, using the atomic force microscope to quantify the role of few-asperity contacts in adhesion." Doctoral dissertation, Worcester Polytechnic Institute, Worcester, MA. February 2006.

[17] Veeco Instruments, "Practical Guide to Scanning Probe Microscopy", www.veeco.com

Appendix A: Derivations of Adaptations to the Force-Balance Method

Initial Approach

Using the conventions established in Figure 35, we begin by summing the forces acting parallel to the tip's orientation.

$$\sum F_{\parallel} = F_z - (F_N - A)\cos\theta - F_f \sin\theta = 0 \tag{1}$$

We then substitute for the force of friction via the Coulomb-Amonton's Law,

$$F_f = \mu(F_N + A), \tag{2}$$

$$\sum F_{\parallel} = F_z - F_N \cos\theta + A\cos\theta - \mu F_N \sin\theta - \mu A\sin\theta . \tag{3}$$

We can then isolate the terms for friction and adhesion,

$$\sum F_{\parallel} = F_z - F_N(\cos\theta + \mu\sin\theta) + A(\cos\theta - \mu\sin\theta) . \tag{4}$$

As this summation needs to equal zero for the forces to be balanced, we see that

$$F_N = \frac{A(\cos\theta - \mu\sin\theta) + F_z}{(\cos\theta + \mu\sin\theta)} . \tag{5}$$

With this relationship in hand, we can move onto the sum of the forces acting perpendicular to the orientation of the cantilever tip,

$$\sum F_{=} = F_X + F_f \cos\theta - (F_N - A)\sin\theta = 0 . \tag{6}$$

Let us substitute the same version of Coulomb-Amonton's Law for the force of friction.

$$\sum F_{=} = F_X + (\mu F_N + \mu A)\cos\theta - (F_N - A)\sin\theta . \tag{7}$$

This can be manipulated to isolate the normal force and the adhesion.

$$\sum F_{=} = F_X + A(\mu\cos\theta + \sin\theta) - F_N(\sin\theta - \mu\cos\theta). \tag{8}$$

At this stage, we substitute for the normal force from (5), and algebraically isolate the lateral force.

$$\sum F_{=} = F_X + \left(\frac{A(\cos\theta - \mu\sin\theta) + F_z}{(\cos\theta + \mu\sin\theta)}\right)(\mu\cos\theta - \sin\theta) + A(\mu\cos\theta + \sin\theta), \tag{9}$$

$$0 = F_X + \left(\frac{A(\cos\theta - \mu\sin\theta)(\mu\cos\theta - \sin\theta) + F_z(\mu\cos\theta - \sin\theta)}{(\cos\theta + \mu\sin\theta)}\right) + A(\mu\cos\theta + \sin\theta). \tag{10}$$

By distributing and collecting like terms, we arrive at a clean final solution.

$$F_X + \left(\frac{F_z(\mu\cos\theta - \sin\theta) + 2\mu A}{(\cos\theta + \mu\sin\theta)}\right) = 0. \tag{11}$$

This is typically referenced as the equality,

$$F_X = \frac{F_Z(\sin\theta - \mu\cos\theta) - 2\mu A}{(\cos\theta + \mu\sin\theta)}. \tag{12}$$

Alternate Derivation

Alternatively, instead of defining theta as above, we can use an angle (φ) which we allow to be greater than 90° for slopes that are down and to the right, as in Figure 35.

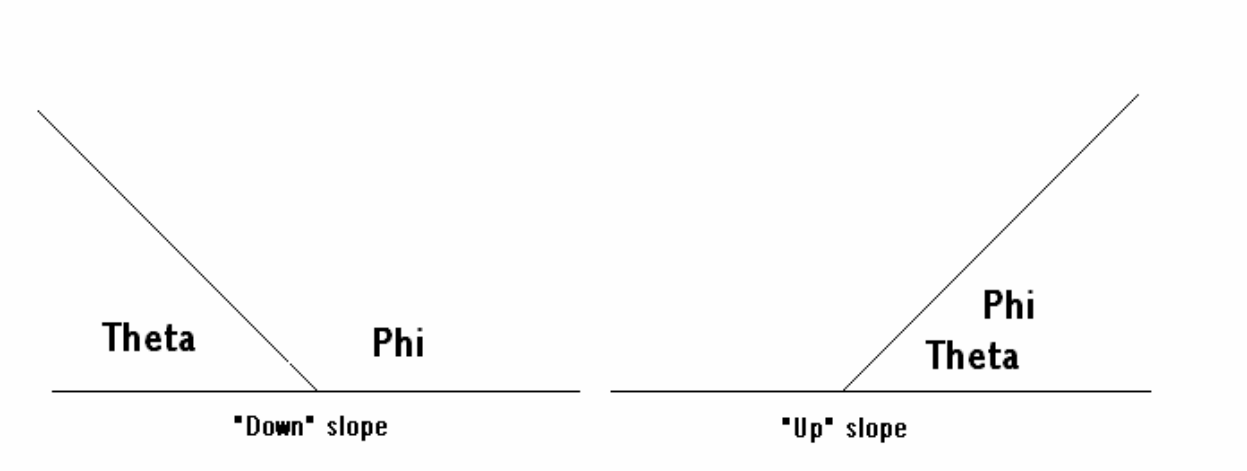

Figure 35: Examples of φ and θ

Using φ instead of θ only changes the cosine terms, since sin(φ)=sin(180- φ)=sin(θ). On the other hand, the cosine terms will be equal (cos(φ)=-cos(θ)) for slopes such as the up slope in Figure 30, and cos(φ)=-cos(θ) for slopes such as the down slope in Figure 30. As such, if looking at an up slope, the equation will be the same for both φ and θ, and for a down slope the only change is one must multiply every cosine term by -1, which leaves us with the exact same format. Thus either method could be used, but for the sake of clarity, this paper will only use the original approach (θ, rather than φ).

Appendix B: Taking Direct Force-Balance Curves on the Veeco Autoprobe M5 AFM

As referenced in Section 4, Data Collection, we reproduced the method proposed by Asay and Kim as best it could be done on the WPI-owned AFM's. Below is a detailed procedure to produce similar data.

1. Begin with standard AFM setup: cantilever mounted, laser adjusted and centered on photodiode, Data Acquisition software opened.
2. Mount sample into AFM. Any stiff, smooth sample of known slope will suffice for the force balance curves, but as the methods require a range of data, calibration gratings are used to provide a range of slopes.
3. Bring tip into contact with the sample.
4. Set scan size small enough to isolate tip motion to one slope.
5. Switch into "Image Mode".
6. Uncheck "Z Servo" box.
7. In the menu bar, go to Setup > Input Config, and add Z Detector and LFM to selected inputs. (Also, add Error Signal if desired). Click [OK].
8. In the menu bar, go to Tools > X-Y Trace.
    a. Set "Driving Signal" to Z Drive.
    b. Default (and maximum) sweep range: -1 to 1
9. Click [Sweep], allow data to be collected, click [Stop].
10. Set "Horizontal Axis" to Z-Detector in drop-down menu. This should redisplay the data.

11. Click [Sweep] to begin collecting data. When the displayed data appears clean, without errors or jumps, click [Stop] to halt data collection. At any point, you may click [Stop] to adjust any of the following parameters before collecting data again.
    a. "Sec", time over which an individual data set is collected
    b. "Points", number of data points per data set
    c. Within driving signal, "From" and "To" may be adjusted to modify the horizontal range of the data.
        i. Decreasing to too small a range can cause chaotic data. If this happens, close X-Y Trace and start over at Step 8.
12. To zoom in one graph, click on the graph and choose the "View One" from the radio buttons at the top. There is no data lost by doing this, only which data is displayed. The original display may be recovered by selecting "View All".

To Save Data

13. Click [>>Clipboard].
14. Open Windows Notepad (notepad.exe).
15. Paste data (Edit > Paste).
    a. Ignore error message. Although data may appear truncated, it is in the file and will be saved.
16. Save file (File > Save).
    a. Ignore error message. Data will be successfully saved.
17. To view raw data, file must be opened in Microsoft Wordpad.
    a. The file is too large for Notepad to view.

18. To analyze data, file may be opened in Microsoft Excel. In the "Text Import Wizard", indicate that the data is of type "Fixed Width" (should be default setting).
    a. Save file in Excel format to preserve any analysis.

Appendix C: Grant Proposal

As AFM research requires many costly supplies, it was important to attempt to gain funding for the project. An application was submitted to the Grants-In-Aid of Research program, administered by Sigma Xi, The Scientific Research Society. This program is designed to offer grants to undergraduate and graduate students, based on the scientific merit of the proposed project, and is highly competitive. Below is the application and budget submitted; we were awarded the full $690 requested to fund our experiment.

Improved Direct Force Balance Method for Lateral Force Calibration

Lateral force microscopy is an important tool in the study of nanotribology. It allows the researcher to quantify the friction as well as other lateral forces in the system. To interpret and use these data, the cantilever's response to a lateral force must be calibrated. Unfortunately, the most prevalent method for this calibration, developed in 1996 by Ogletree, Carpick, and Salmeron, requires repeated scans which can result in wear on the tip, which can prove detrimental to the lateral resolution of the images. An alternative approach has been proposed by Asay and Kim to calibrate the cantilever using direct force-balance equilibrium to eliminate lateral motion, thus minimizing wear on the tip.

The proposed advantages of the direct force-balance method are beneficial to lateral force microscopy, however the derivations and final formulae presented by Asay and Kim ignore key elements in the system. Specifically, the frictional force, adhesion force, and lateral bending of the cantilever were not accounted for when developing the force-balance equations. The addition of these elements to the force balances significantly changes the resulting calculations for lateral force on the cantilever, and thus the lateral calibration factor, implying that there are flaws in the original assumptions.

Within the force-balance system, the mathematical addition of friction changes the functional dependence of the lateral forces on the angle of the scanned surface. Through experimental testing of varied surface angles we will investigate if the calculated lateral calibration factor remains independent of the angle of the scanned surface for Asay and Kim's original method, and for our modified force-balance equations. Since these approaches have different functional dependences on the angle, we expect only one of them will satisfy this condition of angular independence.

The addition of friction presents a challenge in that the system of equations is impossible to solve unless there is a relationship between friction and another force. At the nanoscale the traditional relationship of Coulomb-Amonton's Law does not always apply. For our purposes, we will investigate the interaction and linearity of this relationship on mica, silicon, and graphite samples, to test for the existence of a linear relationship which would allow us to solve the equations.

To benchmark the efficacy of the published method of force balances and our extension of it, they should be compared to the published and accepted method put forth by Ogletree, Carpick and Salmeron. Through this, we can demonstrate the effect of individual assumptions upon the resulting lateral calibration factor.

The practicality of the proposed force-balance systems must be weighted against its accuracy in comparison with accepted means of calibration. Our objective is to improve and validate the force-balance method. This work will be of significant use for further research involving lateral force microscopy by providing an alternate calibration method which causes less wear upon the tip while still finding an accurate lateral calibration factor.

Literature Citations

Asay, D.B., Kim, S.H. "Direct force balance method for atomic force microscopy lateral force calibration" Review of Scientific Instruments, **V 77** (2006)

Ogletree, D.F., Carpick, R.W., Salmeron, M. "Calibration of frictional forces in atomic force microscopy" Review of Scientific Instruments, **V 67**, 3298-3306 (1996)

Mate, C.M., McClelland, G.M., Erlandsson, R., Chiang, S. "Atomic-Scale Friction of a Tungsten Tip on a Graphite Surface" Phyiscal Review Letters, **V 59** No.17, 1942-1945 (1987)

Matei, G.A., Thoreson, E.J., Pratt, J.R., Newell, D.B., Burnham, N.A. "Precision and accuracy of thermal calibration of atomic force microscopy cantilevers", Review of Scientific Instruments, **V 77** (2006)

Budget

From MicroMash:

TGF11 Silicon Calibration Grating (Step angle of 54.4degrees) $200

Known angle necessary for our investigation and comparison to accepted method.

Package of 15 NSC36 triple rectangular cantilevers with AL backside coating

(Force Constants 0.6, 0.95, 1.75 N/m) $300

Cantilevers needed with a range of force constants to verify calibration method on different cantilevers.

From SPI Supplies:

Grade V-1 Muscovite (SPI #01868-CA)

15mm x 15mm x 0.15mm, Package of 20 $41.83

Smooth mica surface necessary to test for linearity of friction and provide a calibration surface

Silicon 100 Wafer (SPI #4136SC-AB) Pre-diced 5mm x 5mm $70.32

Silicon is the most common calibration surface, needs to be tested for linearity of friction

Highly Ordered Pyrolitic Graphite (SPI #429HP-AB)

SPI-3 Grade, 10mm x 10mm x 1mm $77.54

HOPG is atomically flat and may provide a better friction response for lateral calibration

Total Requested: $690

Appendix D: Supplementary Data

Untilted Upslope Scan using NSC12 Cantilever on Beta Scanhead

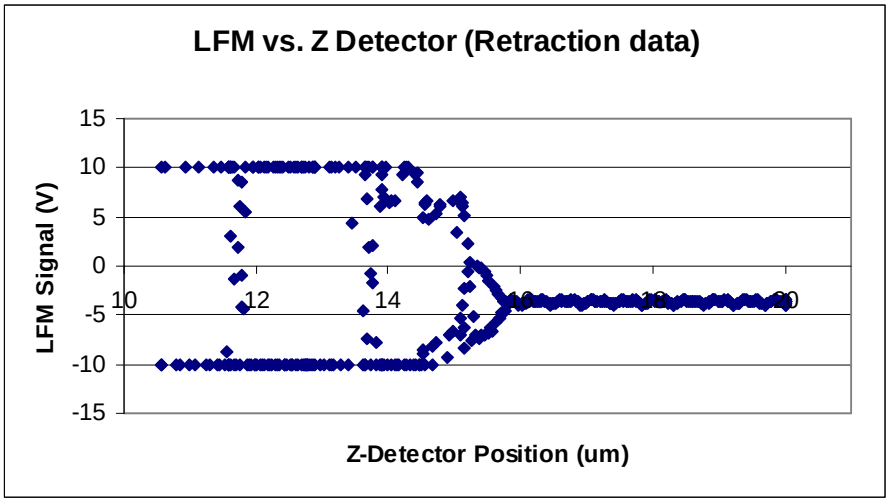

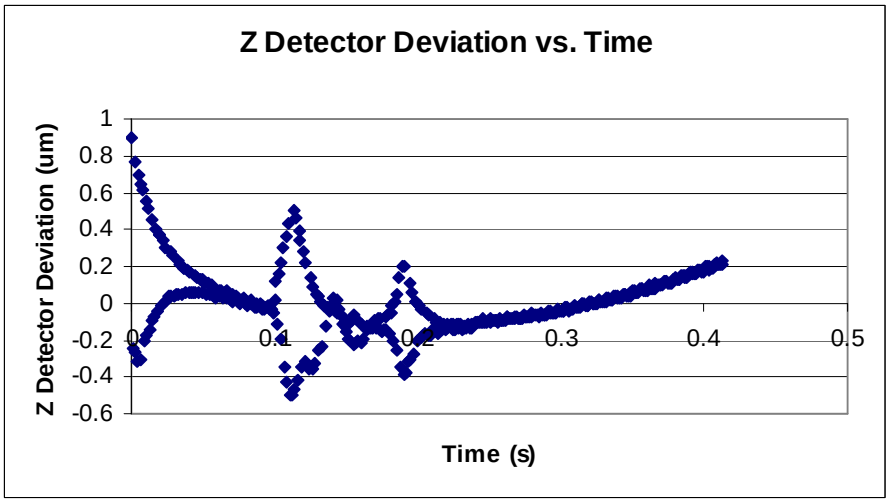

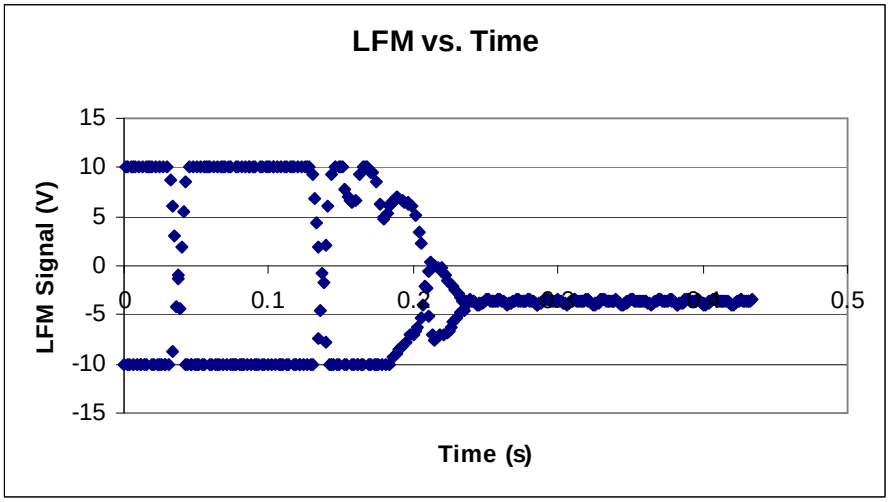

Untilted Plateau Scan using NSC12 Cantilever on Beta Scanhead

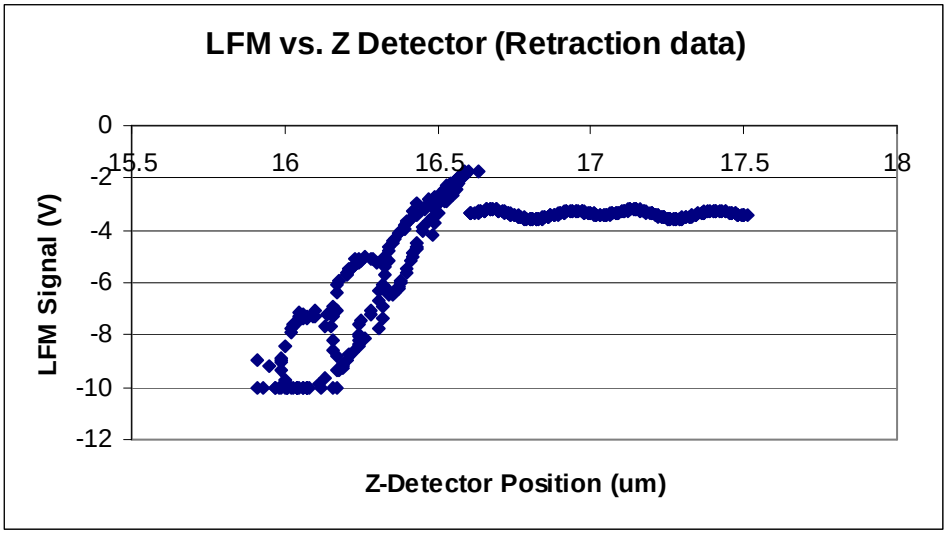

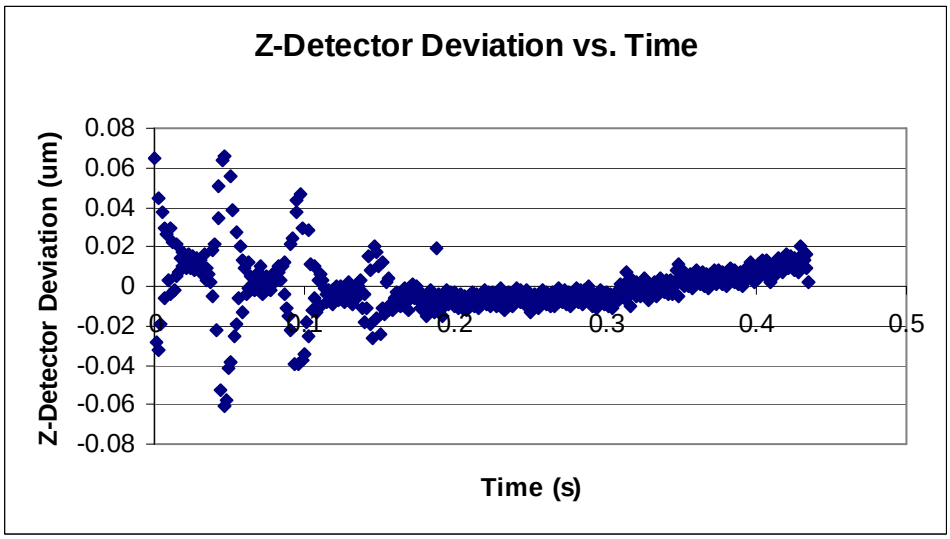

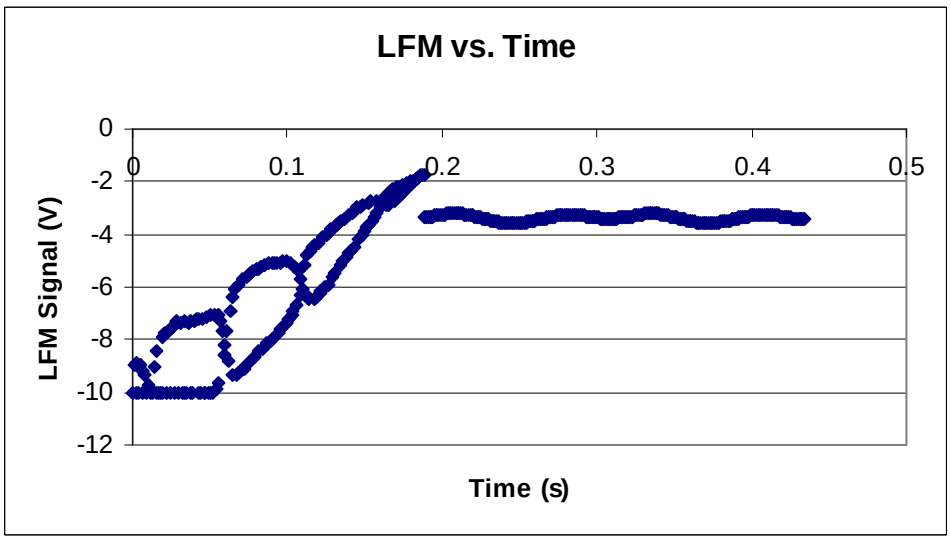

Untilted Downslope Scan using NSC12 Cantilever on Beta Scanhead

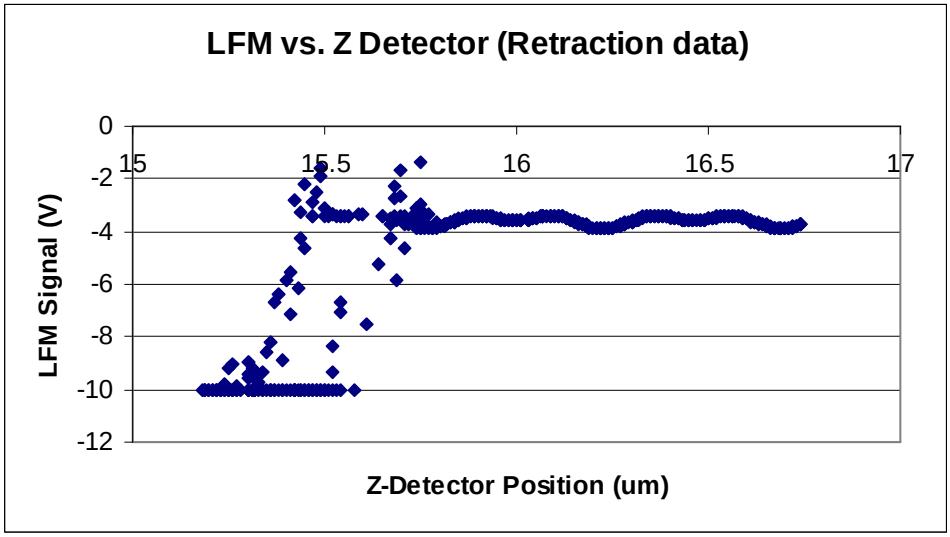

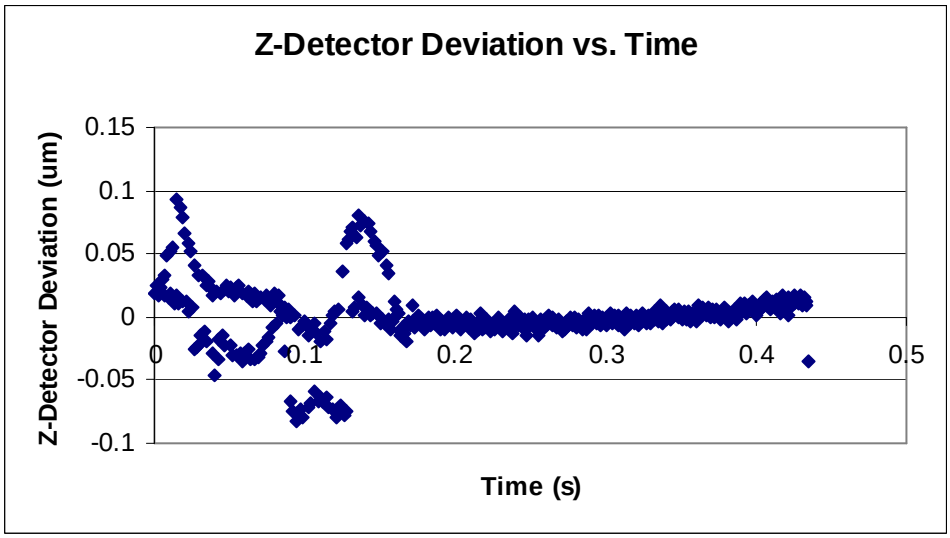

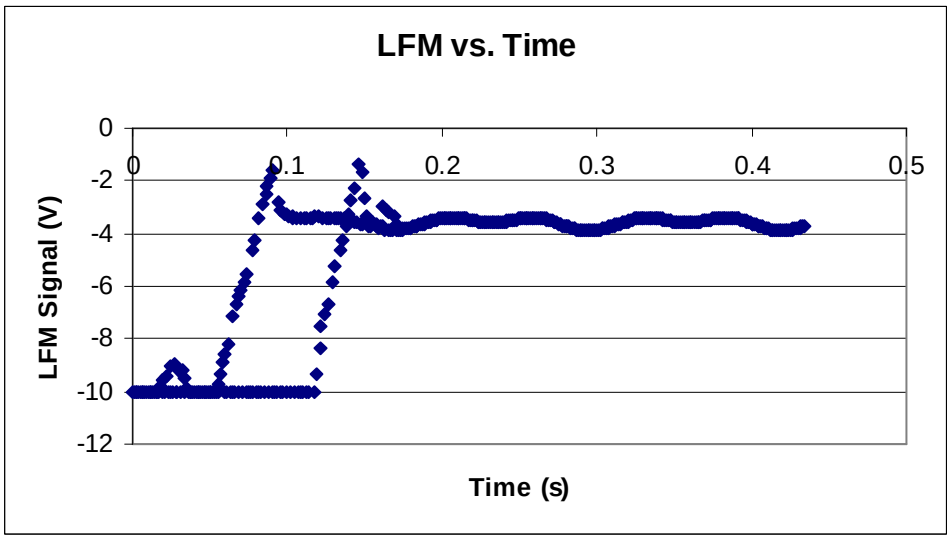

Note: Untilted NSC12 data on Beta scanhead taken from 1-second data runs.

Tilted Upslope Scan using NSC12 Cantilever on Beta Scanhead

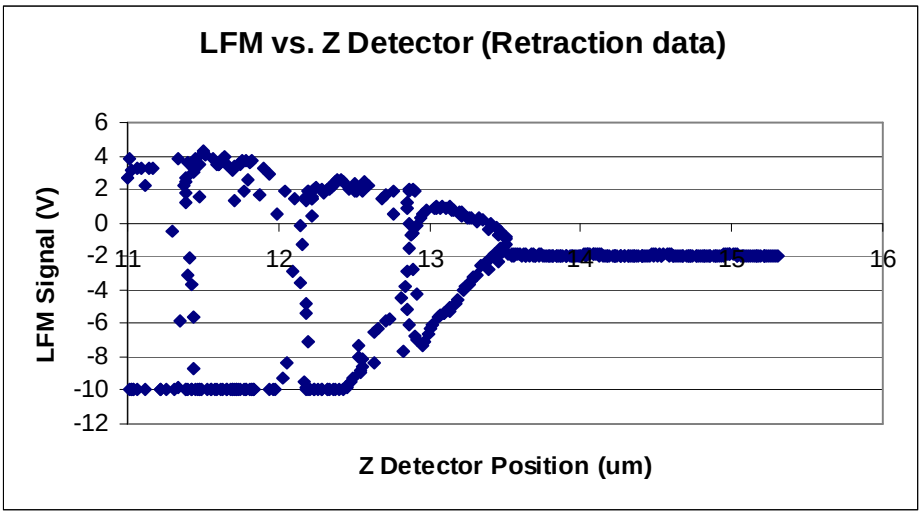

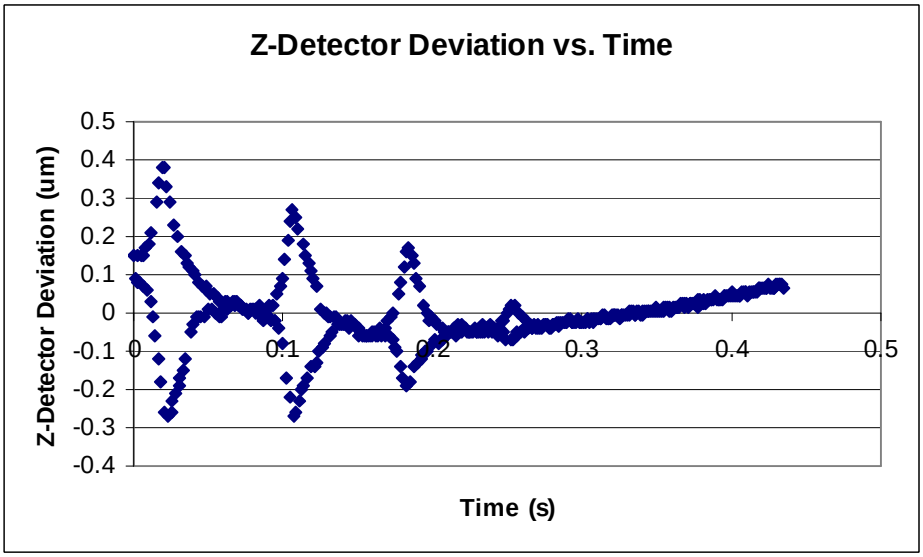

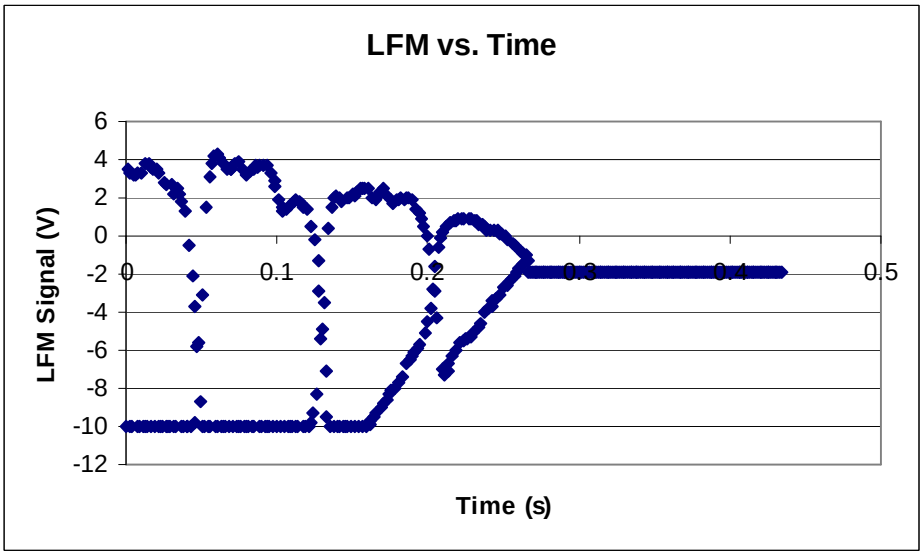

Tilted Plateau Scan using NSC12 Cantilever on Beta Scanhead

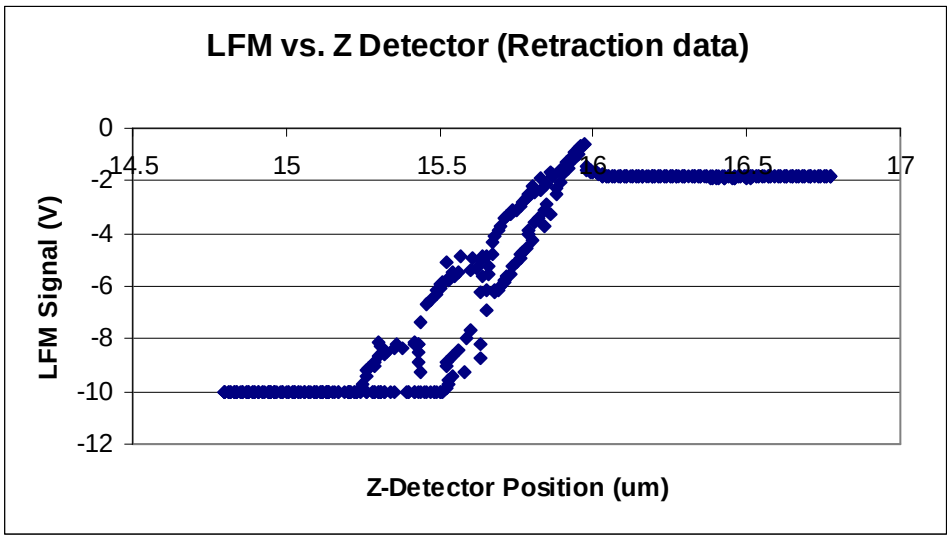

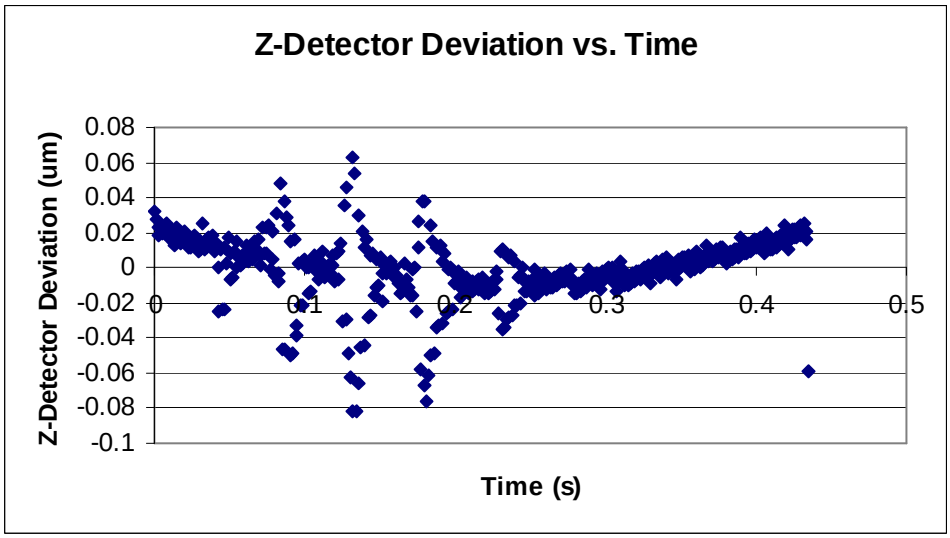

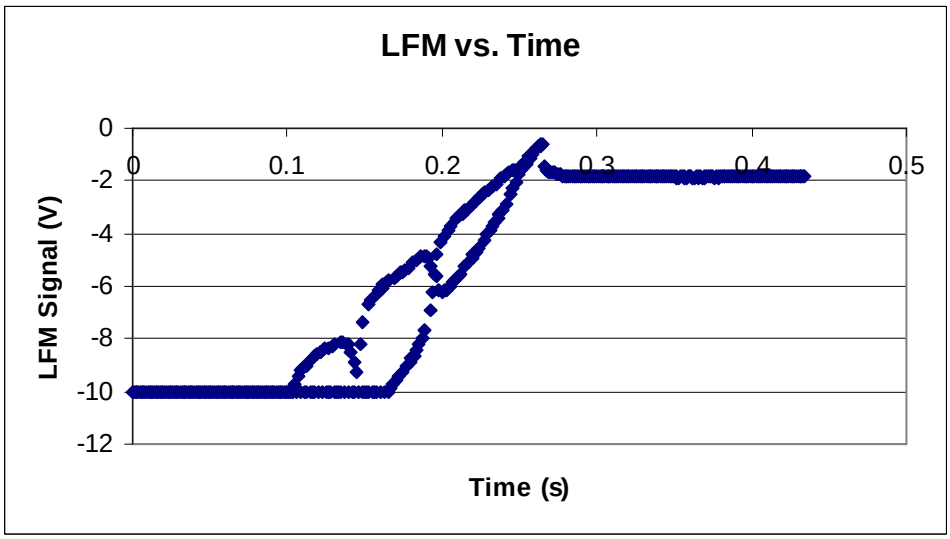

Tilted Downslope Scan using NSC12 Cantilever on Beta Scanhead

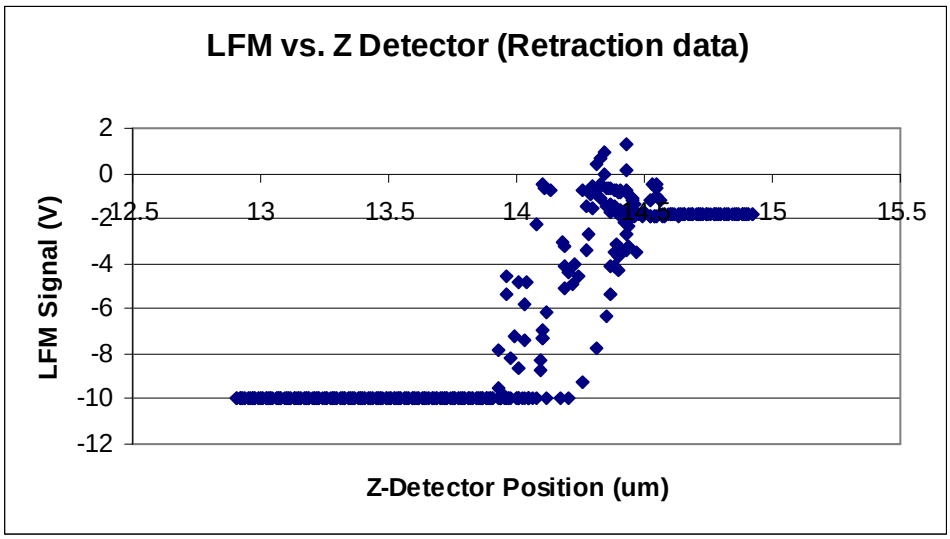

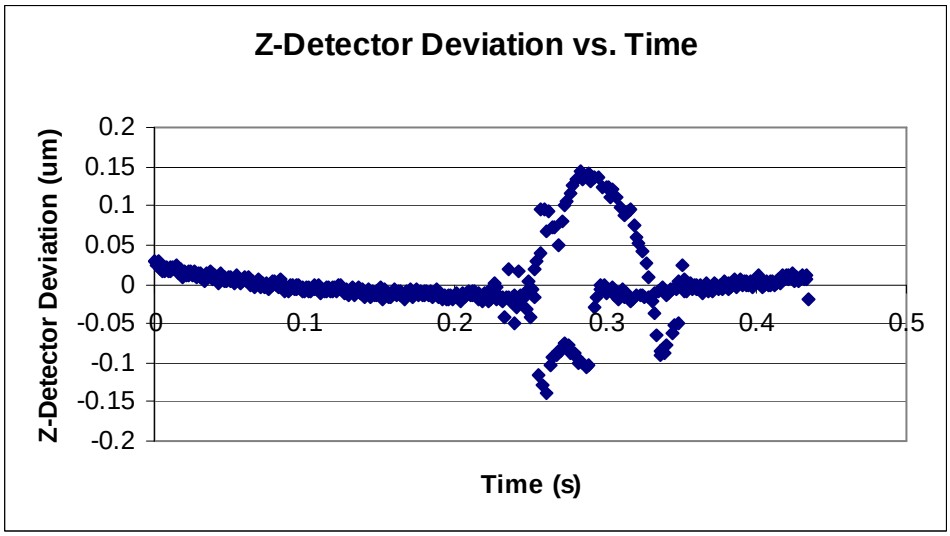

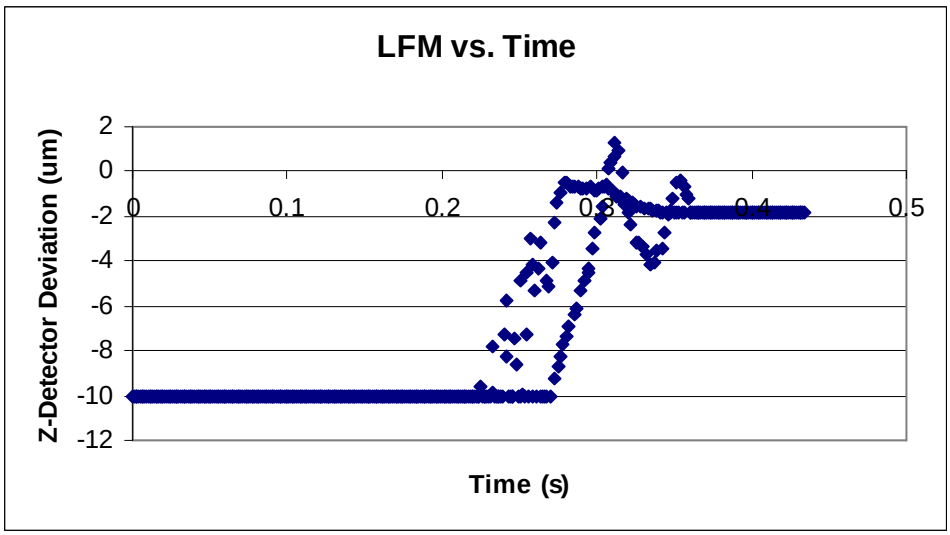

Note: Tilted NSC12 data on Beta scanhead taken from 1-second data runs.

Untilted Upslope Scan using CSC17 Cantilever on Beta Scanhead

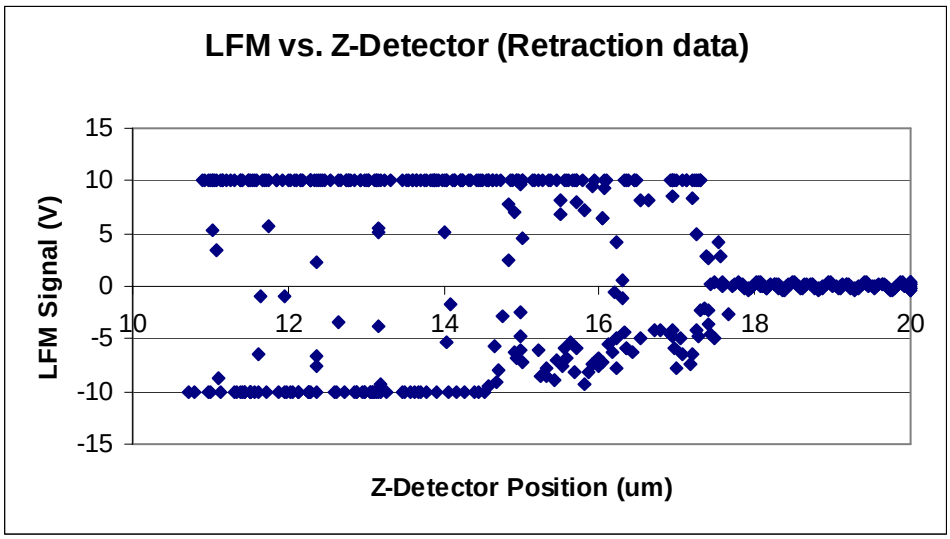

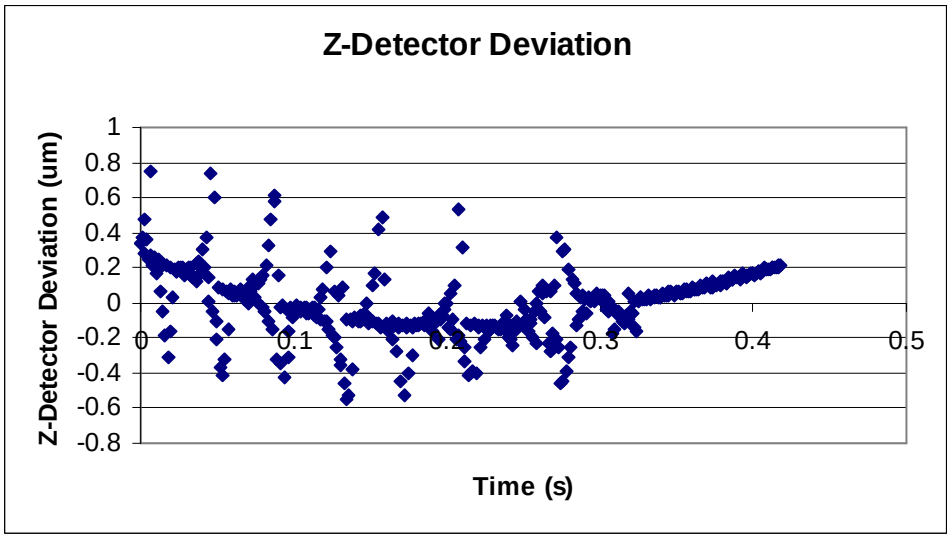

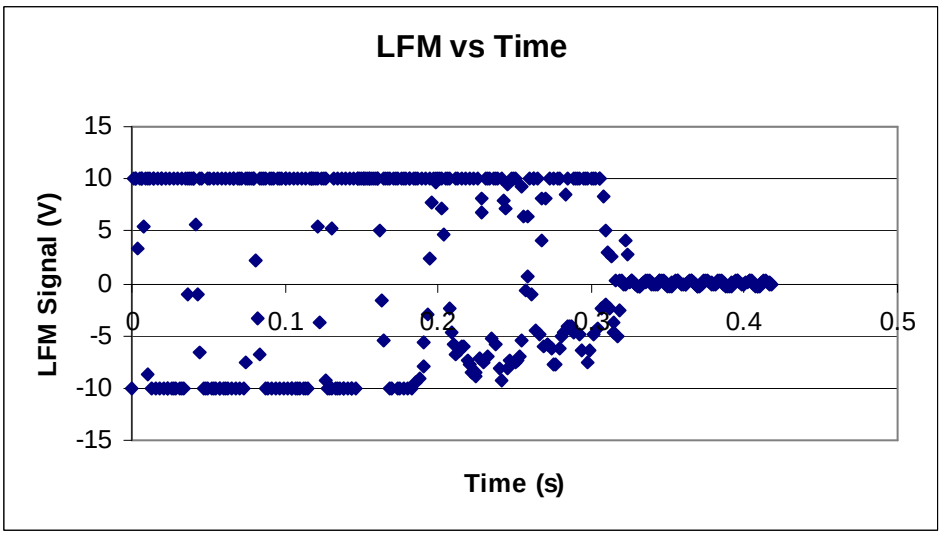

Untilted Plateau Scan using CSC17 Cantilever on Beta Scanhead

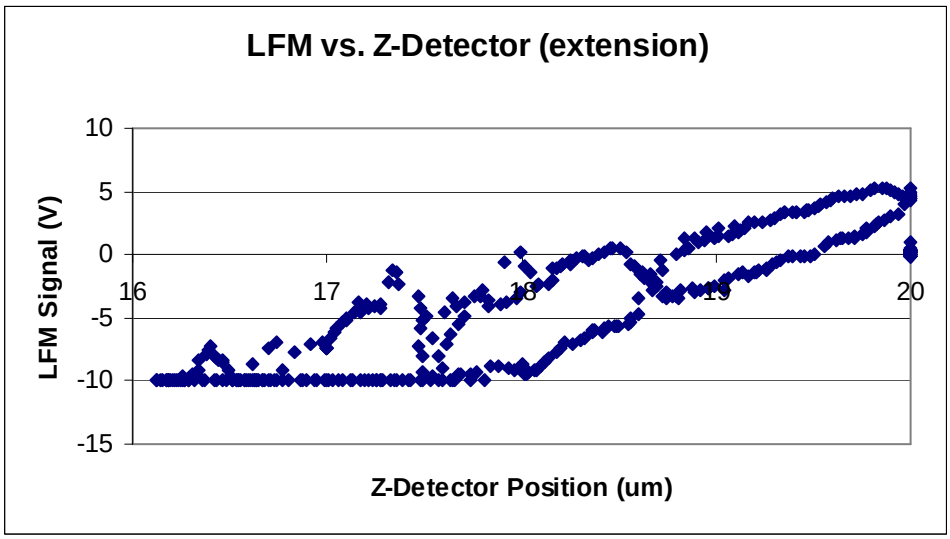

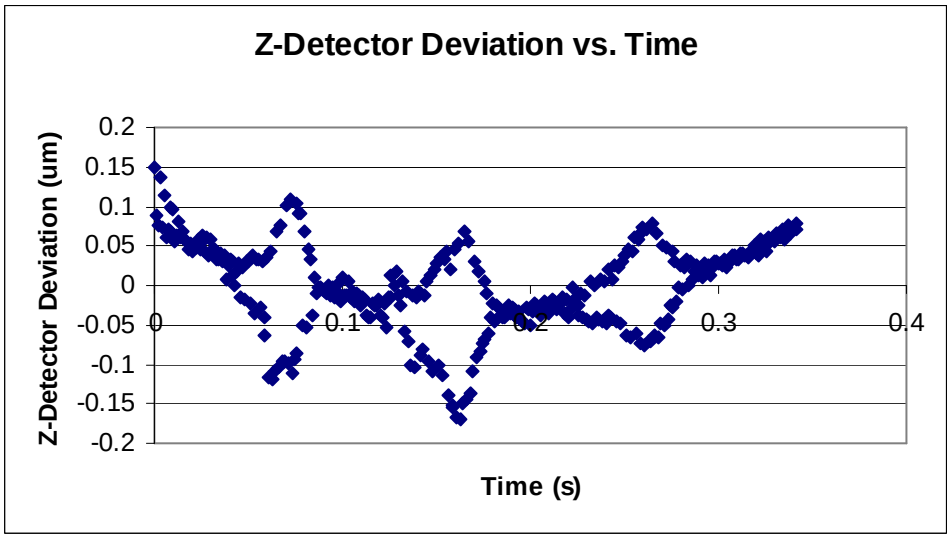

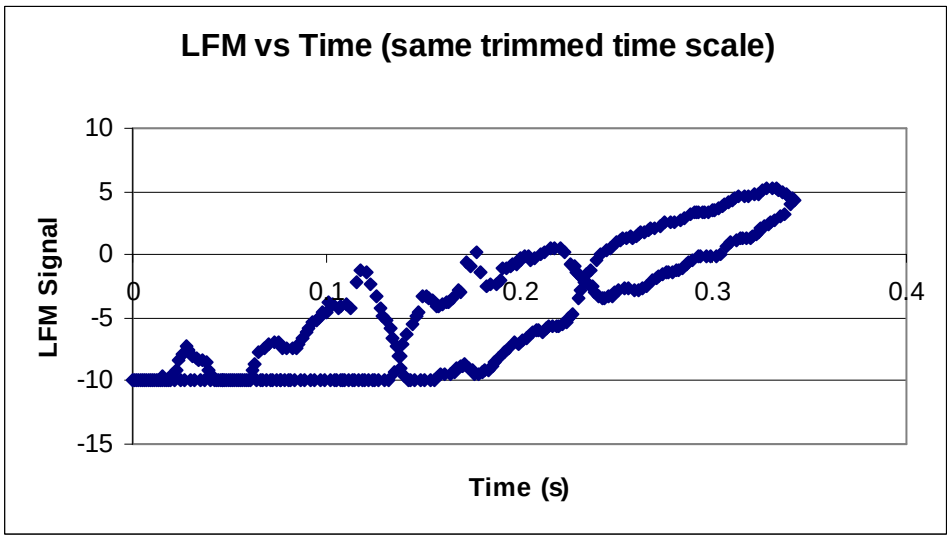

Untilted Downslope Scan using CSC17 Cantilever on Beta Scanhead

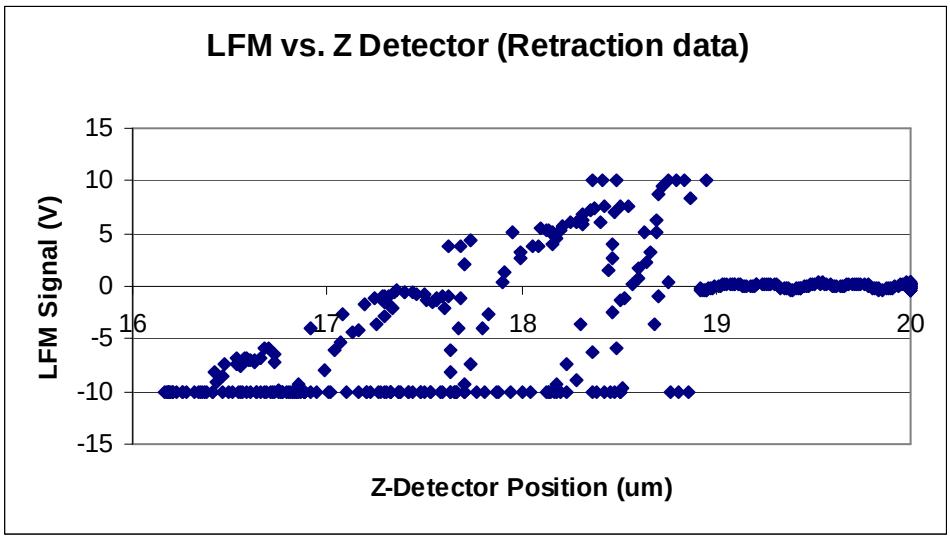

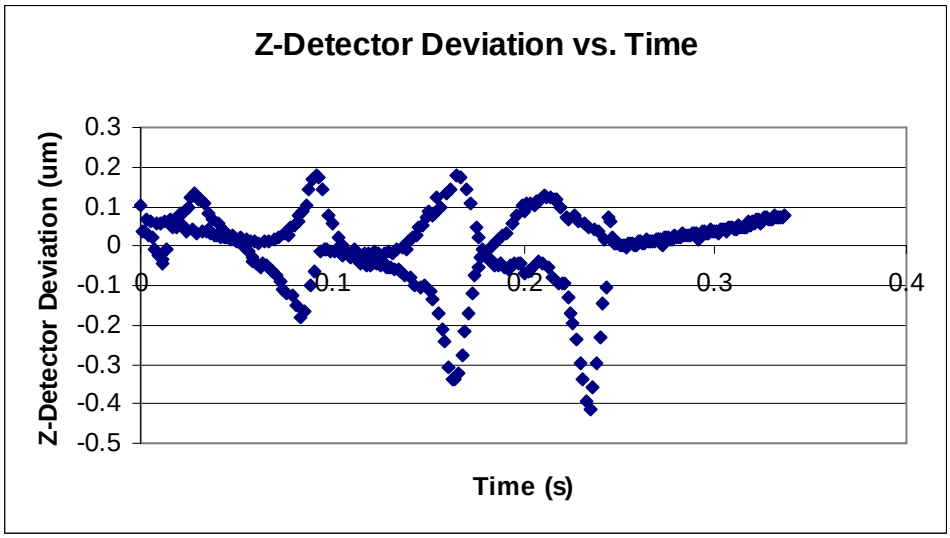

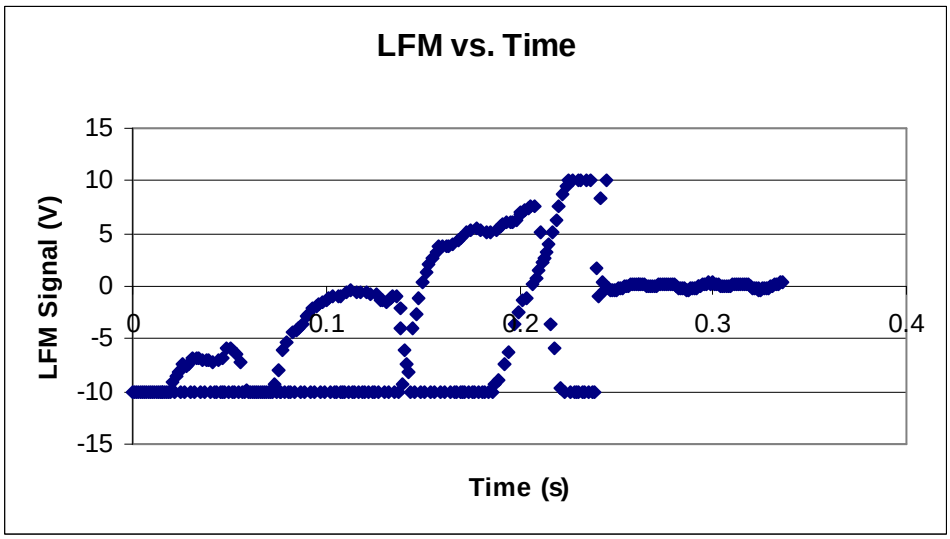

Note: Untilted CSC17 data on Beta scanhead taken from "RUN2" dataset.

Untilted Upslope Scan using CSC17 Cantilever on Alpha Scanhead

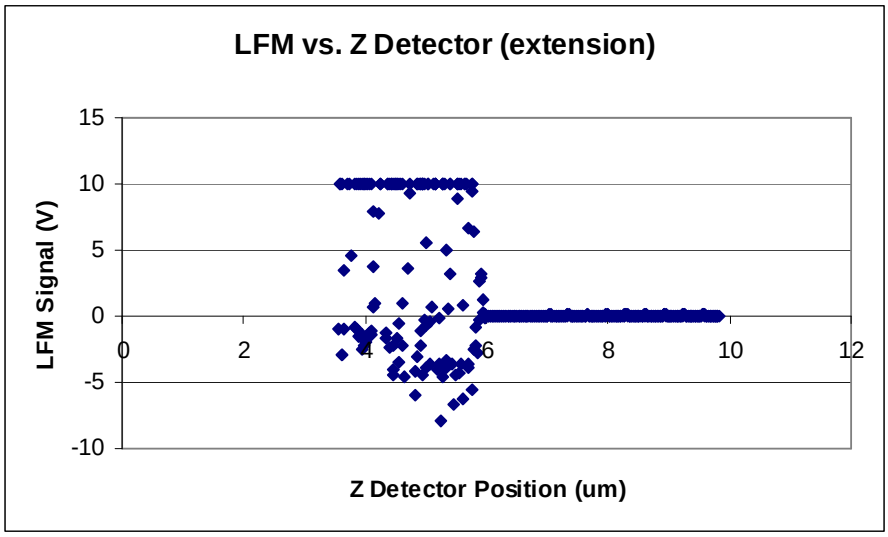

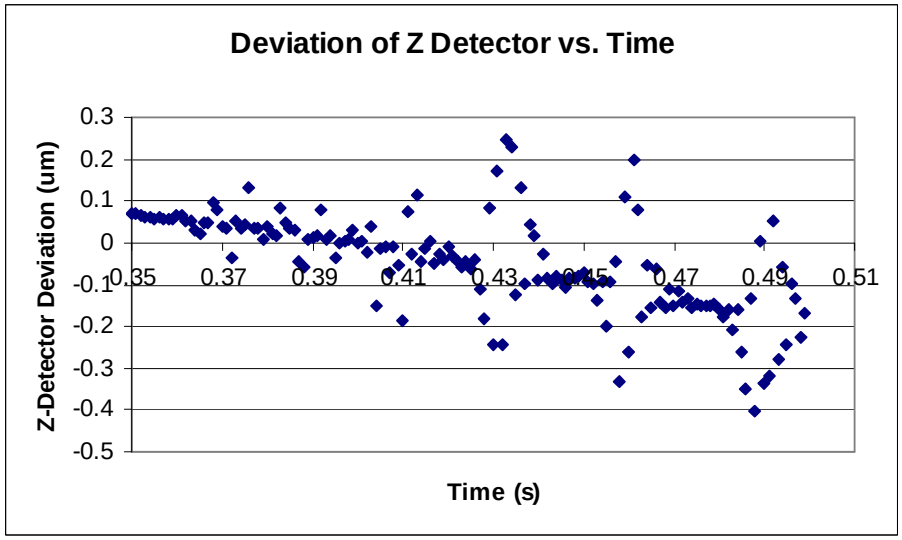

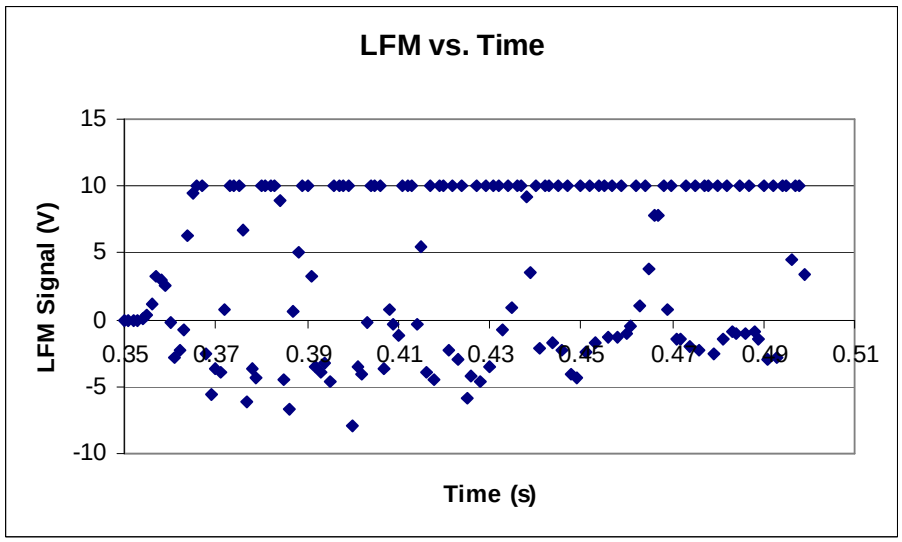

Untilted Plateau Scan using CSC17 Cantilever on Alpha Scanhead

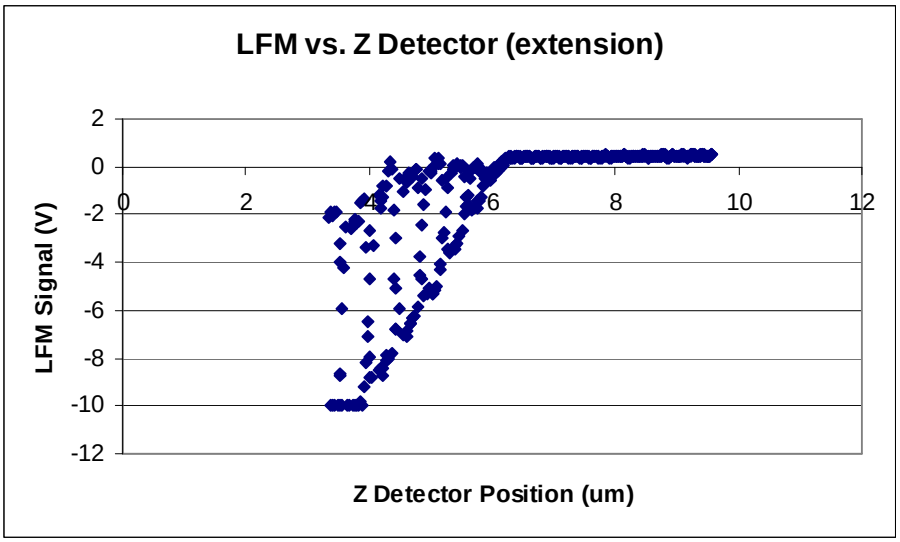

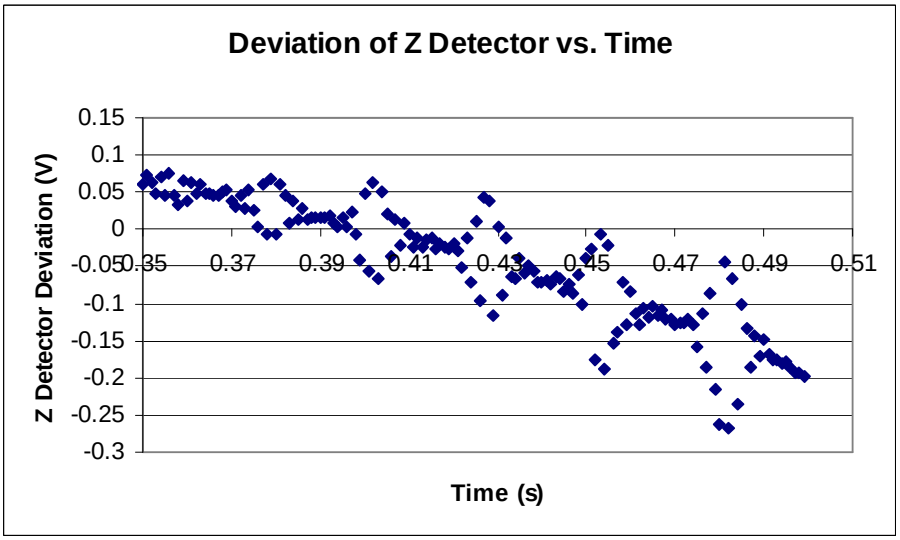

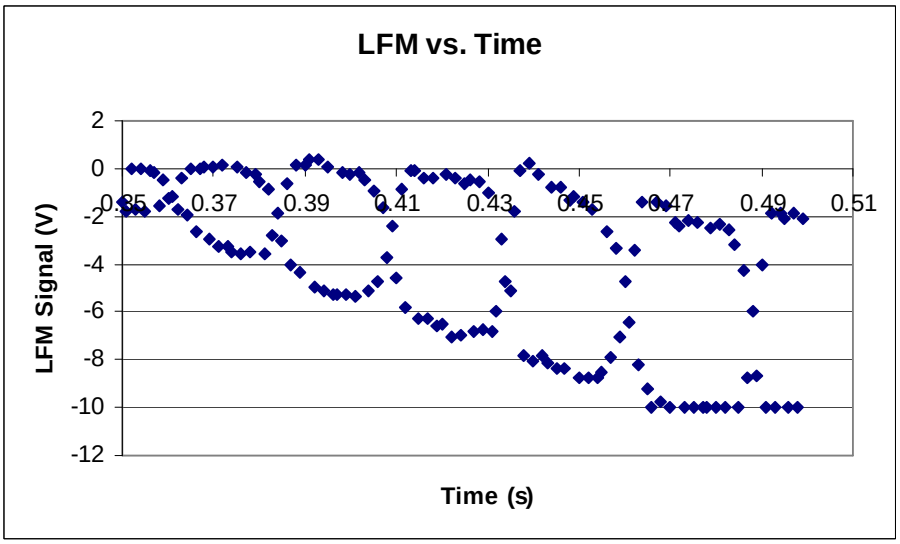

Untilted Downslope Scan using CSC17 Cantilever on Alpha Scanhead

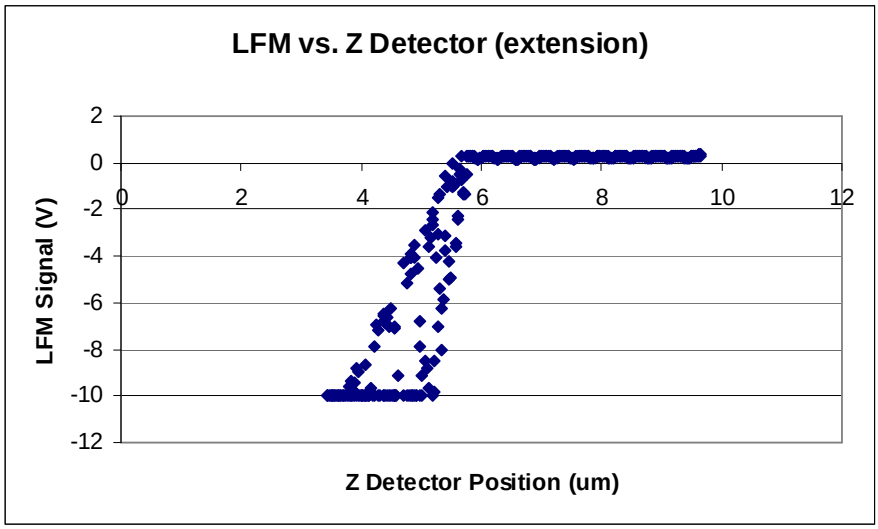

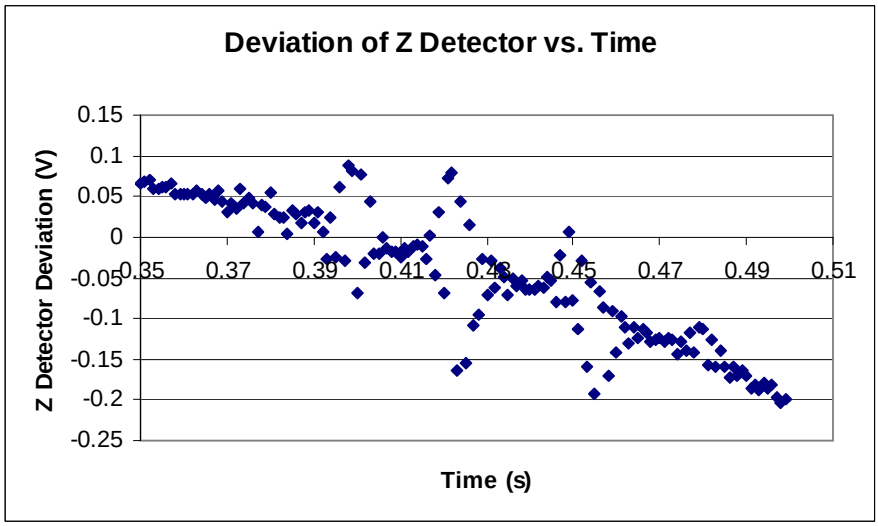

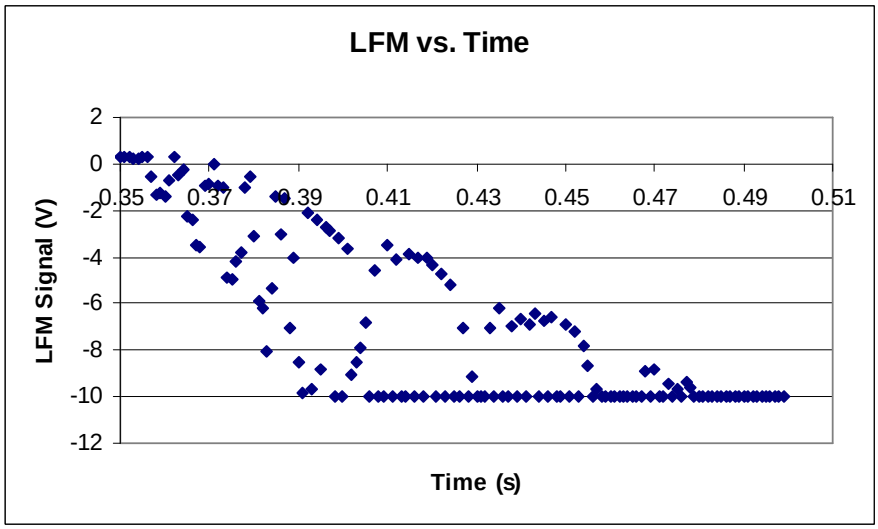

Note: Data taken on the Alpha scans are extension graphs from the non-range-adjusted data.